République algérienne démocratique et populaire
Ministère de l'enseignement supérieur et de la recherche scientifique
Université Saad Dahleb Blida 1

Faculté des sciences
Département de physique

Mémoire de fin d'étude
Pour l'obtention du diplôme de Master en Physique
Option : Micro & Nano Physique

Thème :

Effect of Cu/Ni Ratio on the Chemical composition, Magnetic behaviour, and Structural properties of a FeCuNi based alloy

Présenté par :
KINAI KHAOULA
AMARI NIHAD

Soutenu le 21 /10/ 2021 devant le jury composé de :

Dr. LASLOUNI WARDA	MCB USDB	Président
Dr. OUARAB NOURDINE	MRA CRTSE	Examinateur
Dr. YOUNES ABDERRAHMANE	MRA CRTI	Encadreur
Dr. ABDELKADER HASSEIN-BEY	MCB USDB	Co-Encadreur

Blida 1-2020/2021

ملخص

الهدف من هذا المشروع هو دراسة وفهم تأثير تركيز النحاس والنيكل على الخصائص المغناطيسية والمورفولوجية والهيكلية لسبائك $Fe_{70}Cu_{30-x}Ni_x$.تم تصنيع هذه السبيكة عن طريق خلط مسحوق الحديد والنيكل والنحاس بطريقة الطحن الميكانيكي لمدة 10 ساعات. تم تحديد العناصر المتحصل عليها باستعمال تقنيات مختلفة: الأشعة السينية(XRD)، مجهر المسح الإلكتروني (SEM) وتقنية الاهتزاز المغناطيسي (VSM) .أظهرت الدراسة بالأشعة السينية أن حجم البلورات يتناقص مع زيادة نسبة النيكل. أما بالنسبة للخصائص المغناطيسية؛فلاحظنا تزايد في المقاومة المغناطيسية (Hc) والتشبعالمغناطيسي(Ms) من 83Oe، 121.5emu / g إلى 156Oe، 140emu / gعلى التوالي.

Résumé

Le but de ce projet est d'étudier et comprendre l'influence de la concentration du cuivre et du nickel sur les propriétés magnétiques, morphologiques et structurales de l'alliage $Fe_{70}Cu_{30-x}Ni_x$. La synthèse de cet alliage a été effectuée par le mélange de fer, de nickel et de cuivre par la méthode de la mécanosynthèse pour 10 heures de broyage. Les éléments élaborés ont été caractérisés par des différentes techniques : la diffraction par rayon X (DRX), Microscope Electronique à Balayage (MEB) et le Magnétomètre à Echantillon Vibrant (VSM). L'étude par diffraction des rayons X montre que la taille de la cristallite diminue avec l'augmentation du Ni. Concernant les propriétés magnétiques ; la coercivité Hc et le moment de saturation Ms augmentent de 83 Oe, 121.5 emu/g à 156 Oe, 140 emu/g respectivement.

Abstract

The aim of this project is to study and understand the influence of copper and nickel concentration on the magnetic, morphological and structural properties of the $Fe_{70}Cu_{30-x}Ni_x$ alloy. The alloy was elaborated by mixing iron, nickel and copper powders by the mechanical alloying technique for 10 hours of milling. The elements were characterised by different techniques: X-ray diffraction (XRD), Scanning Electron Microscope (SEM) and Vibrating Sample Magnetometer (VSM). The X-ray diffraction study shows that the crystallite size decreases with increasing Ni. When it come to the magnetic properties, the coercivityHc and the saturation moment Ms rise from 83 Oe, 121.5 emu/g to 156 Oe, 140 emu/g respectively.

Acknowledgment

First and foremost, we must acknowledge our limitless thanks to Allah, for granting us the wisdom, health and strength to undertake this research task.

We express our gratitude to our research supervisors, Dr. Younes Abderrahmane and Dr. Abdelkader Hassein-Bey, for rectifying our vision and for their support and guidance during every moment till this paper is finally able to see light.

We would also like to thank all the jury members, Dr.Laslouni Warda and Dr.Nouredine Ouarab, for being here with us to review this work.

Last but not the least, we would like to thank our parents for their support, love, confidence. Without you, none of this would indeed be possible.

Dedication

I dedicate this work to:

My parents who raised me with love of science and provided me so much support…

My sisters and my dear cousin Amira who encouragedme and supported me …

And to my partner Khaoula.

Dedication

I dedicate this work to my parents and my brothers and sisters specially to my brother Abbdrrahmen who was my driver during my internship days, and to my friend Warda who was my mental supporter, and to my partner Nihad.

List of figures

Content table

GENERAL INTRODUCTION

GENERAL INTRODUCTION

Nanomaterials are a new class of materials that have at least one dimension in the range of 1-100 nanometre [1]. Due to quantum confinement effects, the morphological, electronic, optical, magnetic, and chemical characteristics of these nanomaterials improve significantly when their size decreases to the nanoscale range, which makes them attractive for various emerging applications [2, 3]. Nanomaterials have recently emerged as one of the most active research fields in the field of solid-state physics, serving as an inspiration to many individuals and research groups around the world. This was due to the need to fabricate new materials on a finer scale in order to continue lowering costs while increasing the speed of information transmission and storage. Another advantage of nanomaterials is that they have novel and often enhanced properties when compared to traditional materials, which opens the door to new technological applications.

A variation of the elaboration technique was employed in the production of these components. We have opted for mechanical alloying as the elaboration method for this project. The Mechanical alloying process has gotten a lot of attention because it can be used to make a variety of advanced materials, including non-equilibrium, and composites [4, 5]. As a result, this method can produce alloys and compounds that are difficult or impossible to acquire with conventional melting and casting [6].

The combination of Fe, Ni, and Cu allowed us to study the impact of the copper on the FeNi system alloy. Some researchers found that when the copper is associated with nickel, it allows good sinterability of the powder [7] and improves its hardening in reactor pressure vessel steels used in existing nuclear power plants [8].

The presence of Ni promotes the nucleation of Cu precipitates and it has some influence on coarsening rate, which indicates that Ni atoms accelerate Cu diffusion in ferric alloy. During the formation of Cu precipitates in the Fe matrix, the Cu atoms and Ni atoms interact with one another. There are three different stages of the diffusion of Cu, based on the various interactions of the nickel and copper atoms. The first stage is for the free diffusion of Cu and Ni atoms. In this stage, the Ni atoms can visibly enhance the Cu precipitation. The second stage involves the mutual promotion of Ni and Cu atoms. As for the third stage, it is for the inhibition of Ni atoms on Cu diffusion. Cu and Ni form tiny clusters that develop into bigger ones, behaving as precipitation precursors. [9, 10].

The aim of this work is to produce a powder alloy based on Fe,Ni and Cu using the mechanical alloying technique, then study their morphological, structural, and magnetic

properties. The structural characterization and phase transformations of the obtained powder mixture are studied by X-ray diffraction. The magnetic properties are determined by vibrating samples manometers (VSM).

There are three chapters in this thesis. The first chapter is a general overview of nanomaterials, including their structural properties, classification, and description of spray coatings and their techniques.

The second chapter provides general information about the alloy as well as the main research works about it, as well as illustrations of the experimental methods and characterization techniques used, such as scanning electron microscopy (SEM), X-ray diffraction (XRD), and magnetometer measurements with a vibrating sample (VSM).

The third chapter and the final chapter describe the various Fe-Cu-Ni alloy results and their interpretations.

Finally, a general conclusion that summarises the main results obtained in this research work and gives perspectives on future work that may be carried out.

CHAPTER 1: NANOSTRUCTURED MATERIALS AND THEIR APPLICATION FIELDS

1. Nanostructure material and their application field

1.1. Introduction:

Nanotechnology is the study and control of matter at the atomic and molecular levels. A new scientific discipline uses the concept of nanometre scale phenomena to create materials and devices with novel properties. It entails the study of nanomaterials, their synthesis, characterization, and applications in all areas of technology. In this chapter, we are going to define briefly whatnanomaterials are and present their history, classification, and main applications in different fields of science and industry. Then we are going to illustrate the various synthesis techniques and provide more details about the mechanical alloying since it is the technique used in this project. Finally, we have dedicated a part to describe the spray coating technique, which has been used as an application of the alloy.

1.2. Nanomaterial:

1.2.1 History:

Over the past few decades, the word “nanomaterials” has become a popular buzzword in journalism and publishing, giving the impression of a new type of technology that has yet to be developed. Nanomaterials are not new at all, and most people are not aware of them [11]. Volcanic ash, sea spray, and smoke are examples of nanoparticles found in nature. Nanomaterials have been manufactured since the 4th century. An example of Roman nanotechnology is the Lycurgus Cup, a glass cup with nanoparticles of gold and silver. Alchemists used nanoparticles to build gold nanoparticle stained glass windows as early as the 1600s.

Even though the employment of nanostructured materials in practical applications has been since the beginning of civilization, it has only been possible in recent years to synthesise these structures in a controlled manner in order to characterise them and gain a better understanding of past and newly discovered nanostructured materials. Over the years, Michael Faraday synthesised colloidal gold solutions in 1857, Nario Taniguchi developed nanometre-precision production techniques in the late 1960s, and IBM introduced the scanning tunnelling microscope (STM) in 1981. The discovery of nanostructure materials has evolved in tandem with technological advancements in their production and characterization. Using carbon as an example, new discoveries in recent years include fullerenes in 1985, carbon nanotubes in 1991, and graphene in 2003 [12].

Nanomaterials are a growing class of materials. In the early 20th century, tyre manufacturers used carbon black to reinforce car tyres (e.g., abrasion resistance, tensile strength) and to help disperse heat load.

Recent research on nanomaterials has attracted a lot of media attention. Nanomaterials enable things to be lighter, tougher, and more aesthetically pleasing while remaining more economical. As a result of faster computers, cleaner energy production, targeted pharmaceuticals, and better construction materials thanks to nanomaterials, the impact of nanomaterials on improving the quality of life is clear [13, 14].

1.2.2. Definition:

There are two ways to define nanomaterials; the firstdefinition states that nanomaterials are materials with individual building blocks that are less than 100 nm in at least one dimension (figure1.1). This definition is well suited for numerous research proposals that commonly prioritise nanomaterials. The second definition is much more restrictive, stating that nanomaterials have properties that are inherently dependent on their small grain size. Given that nanomaterials are typically quite expensive, such a restrictive definition makes more sense [15].

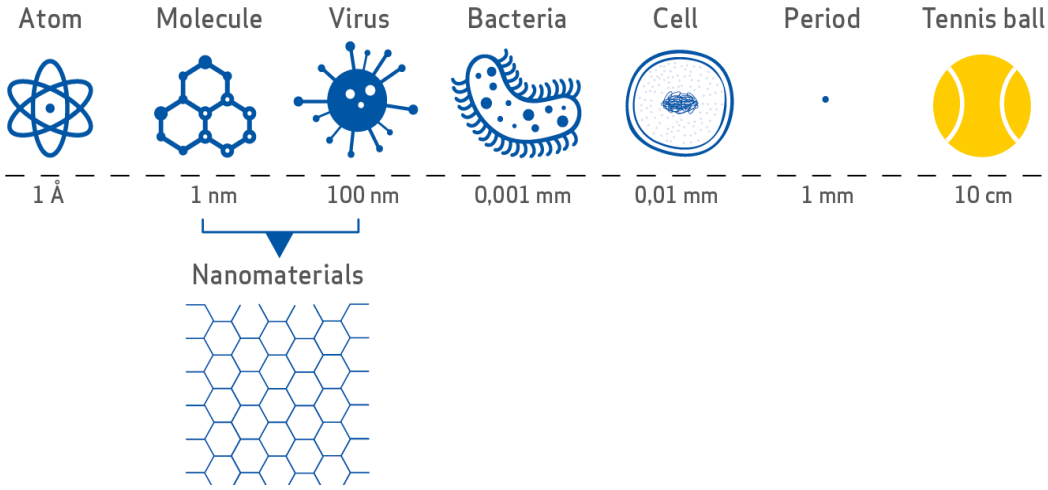

Figure 1.1. Examples of objects manufactured or present in nature in a scale of size in nanometres

1.2.3. Classification of nanomaterials:

Based on the dimensionality of their nanoparticles, there are four classes for nanomaterials: 0-D, 1-D, 2-D, and 3-D (figure 1.2) [15]:

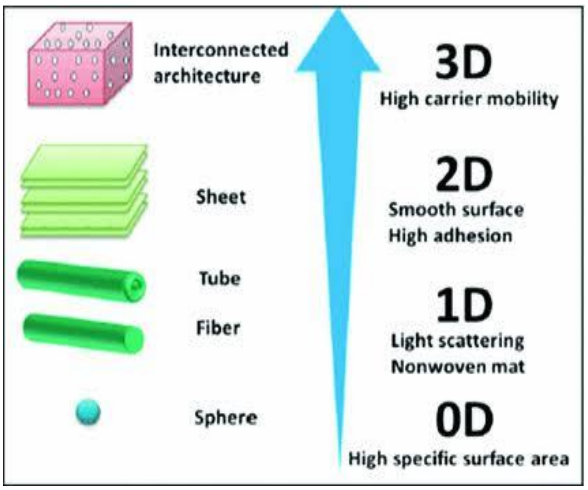

Figure 1.2. Nanomaterial classification

a) 0-D nanomaterials: They are all negligibly small in all three dimensions. Because their energy levels are discrete, they are also known as artificial atoms (or quantum dots). Metallic nanoparticles include gold and silver nanoparticles, while semiconductor nanoparticles include CdS, CdSe, and CdTe quantum dote. Nanoparticles with sizes ranging from 1-50 nm can have spherical, cubic, or polygonal shapes. Fullerence is the most common example, as identified by Kroto and colleagues.

b) 1-D nanomaterials: They have two dimensions of particulates on the nanometre scale, and the third dimension is significant in comparison to the other two dimensions. That is, they have lengths of several micrometres (or>100 nm) and diameters of a few nanometres. Nanotubes, nanofibers, nanorods, or whiskers of metals or oxides, as well as carbon nanotubes (CNTs) and carbon nanofibers (CNFs), are examples. These entities have a large surface area and aspect ratio, making them useful in nanocomposites.

c) 2-D nanomaterials: They have one dimension measured in nanometres, and the other two dimensions are significantly larger than the third dimension (i.e., thickness). Graphene, nanolayers, nanoclays, nanosheets, nanofilms, platelet-like structure, nanoflakes or nanoplatelets, and silicate nanoplatelets are some examples.

d) 3-D nanomaterials: The dimensions of these materials are all outside the nanometre range. Equiaxed nanoparticles or nanocrystals are other names for them. The best example is the nanostructured bulk, made of individual blocks ranging in size from 1 to 100 nm. 3-D nanomaterials are also referred to as “bulk nanomaterials” because they are not restricted to the nanoscale in any dimension. All three dimensions

of these materials are greater than 100 nm. These materials have a nanocrystalline structure of nanoscale features, i.e., bulk nanomaterials are made up of multiple arrangements of nanosized crystals, typically in different orientations. In other words, 3-D nanomaterials can have nanoparticles, nanowires, nanotubes, or multinanolayers dispersed throughout the matrix.

1.2.4. Application of nanomaterial:

Nanomaterials represent an active field of research but also a fast-growing economic sector with a wide range of applications (Figure 1.3). Nanomaterials have undergone a huge evolution recently, mainly for the purpose of miniaturisation. In the field of microelectronics, this has brought considerable advantages, not only in terms of reliability and complexity of the products, but also in terms of cost. As a result, microelectronics has become important in several areas where this was not necessarily expected. Miniaturisation research has also led to the discovery of nanoscale objects such as carbon nanotubes that already have so many applications like: improvement of mechanical resistance (tennis rackets), an additive to resins to render them conducting, electron emitting cathodes, high efficiency gas absorption [16,17]. So many applications of nanomaterials can also be found in the medical and biological domains, from diagnosis and screening to treatment and regenerative medicine.

We can distinguish that different forms of nanoparticles have been developed: spherical (liposomes, micelles, polymeric nanoparticles, nanocapsules, inorganic such as gold and silver, dendrimers, metal-organic hybrids, albumin-based), tubular (carbon, titanium oxide) in order to guarantee the fluid delivery of therapeutic or diagnostic agents to the targeted area [16]. In the field of diagnostic imaging, for example, superparamagnetic nanoparticles based on iron oxide are used in magnetic resonance imaging (MRI).In contrast to paramagnetic products, these particles have no magnetic properties outsideof an external magnetic field [18], and in many other cases, iron oxide particles are used in SPIO (Superparamagnetic Iron Oxide) for the detection of hepatic lesions. After intravenous administration, products such as ferumoxide (Endorem, Feridex) or ferucarbotran (Resovist) are rapidly taken up by the Küpfer cells, causing the lowering of the MRI signal in healthy tissue, SPIOs increase the contrast between healthy tissue and pathological tissue such as cancer [19, 20]. As for the treatment of cancers, nanoparticles spread through the permeable vessels of the tumours, allowing extravasation into the tumours without entering the bloodstream [18].

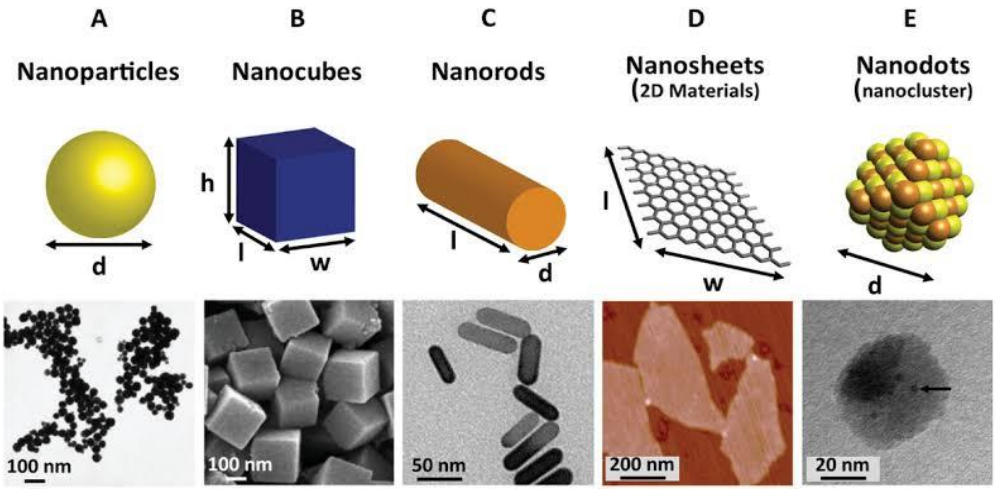

Figure 1.3. Nanomaterials examples

The table 1.1.Shows the main applications of nanomaterials by type, in different fields:

Table (1): nanomaterial applications by type [21]

Nanomaterial	**Domain of application**
Nanoceramic	Structural composites, anti-UV components, mechanochemical polishing of substrates (wafers) in microelectronics, photocatalytic applications
Nanomaterials	Sectors of antimicrobial and/or catalysis, conductive layers in displays, sensors, or energy
Nanoporous	Aerogels for thermal insulation in the fields of electronics, optics and catalysis, bio-medical field for applications such as vectorisation or implants
Nanotubes	Electrically conductive nanocomposites, structural materials - single-walled nanotubes for applications in electronics
Solid nanomaterials	Hard Coatings, structural components for the aerospace, automotive, oil and gas, sports, and anti-corrosion industries oil and gas industry, anti-corrosion
Dendrimers	Medical field (drug delivery, rapid detection), cosmetic field
Quantum dots	Optoelectronic applications (displays), photovoltaic cells, inks and paints for anti-counterfeiting applications, anti-counterfeiting marking

1.3. Nanomaterials synthesis techniques:

There are several methods to create nanomaterials. There are two approaches to create such materials, the bottom-up and the top-down approaches [22]. Using a top-down approach, nanomaterials are created by shrinking bulk materials, while using a bottom-up approach, nanomaterials are created by synthesising atoms and molecules. Top-down approaches involve the attrition (wear) of the source materials, whereas bottom-up approaches begin with

either a solution or a vapour of atoms, molecules, or a precursor that reacts to form the nanomaterial population (figure 1.4), [23].

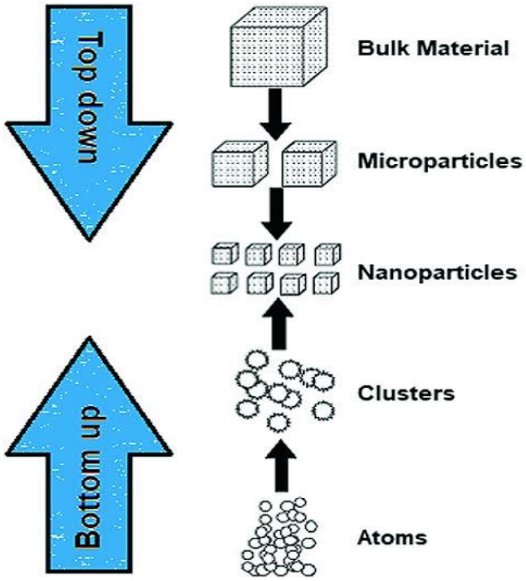

Figure 1.4. Bottom-Up and Top-Down approach

1.3.1. Bottom-up approach:

a) Arc-Discharge:

In the arc-discharge synthesis of nanomaterials, an electrical discharge between two electrodes generates plasma, then vaporises the electrode material[22]. The arc discharge method uses, either gas (as in the generation of CNTs) or liquid-phase systems (as for silver nanoparticles) [24].

b) Inert-Gas condensation:

In Inert-Gas condensation, metal atoms evaporate into an inert carrier gas at a high temperature [25]. Cooling the gas produces supersaturated vapour, and particles nucleated homogeneously in the gas stream from this vapour. Clusters of particles develop and sinter before further cooling the gas, known as the quench gas, or with a chilled surface, which stops both nucleation and sintering [25].

c) Flame synthesis:

Flame synthesis is the most common method for producing commercial quantities of nanomaterials [26]. The process of flame synthesis begins with the evaporation of a precursor, which is then introduced into a stream of inert gas [27]. Before injecting the gas into a flame, we blend it with fuel and an oxidising agent.

d) Vapour-phase deposition:

In nanoparticle synthesis, two types of vapour-phase deposition are used: chemical vapour deposition (CVD) and physical vapour deposition (PVD) [28]. Both methods entail depositing vapour phase materials, which then coalesce to form the desired nanomaterial. A precursor gas is passed over a substrate in a furnace, where it chemically reacts with the surface, depositing the desired chemical species and resulting in the formation of the nanomaterial. While CVD involves a chemical reaction between the precursor and the substrate, PVD deposits the material through a purely physical process with no chemical reaction [29].

e) Colloidal synthesis:

It is common to reduce metal complexes in dilute solutions in order to obtain colloidal dispersions of metal nanomaterials [30]. The reduction reaction leads to the creation of a supersaturated solution of metal atoms, which then nucleates [30].

f) Biologically synthesised nanomaterials:

A wide range of microorganisms, including bacteria, fungi, actinomycete, and viruses, can synthesise nanomaterials. Synthesis can occur inside or outside of biological cells (intracellular or extracellular) [26].

g) Microemulsion synthesis:

Micelles (or reverse micelles) can make nano materials [31]. It may be possible, for example, to create micelles containing the two precursors required for nanomaterial growth and then allow them to collide with each other. This method of synthesis does seem to be well suited for the production of nano materials with a "core-shell" structure; that is, nano materials with a core made of one material surrounded by a shell made of a different material [32].

h) Sol-Gel method:

As the name implies, this method begins with the formation of a colloidal suspension, known as the sol, and then gels the sol to form an inorganic network in a continuous liquid phase, known as the gel. A wet-chemical technique begins with the hydrolysis of a precursor, typically metal alkoxides (to form metal oxide clusters). Then followed by a condensation reaction, such as polycondensation or polyesterification [33], which causes the solution's viscosity to increase. By adjusting the reaction conditions, we could controlthe size and morphology of the formed nanoparticles. As a result of an incomplete reaction, organic groups may be included in the nanomaterial. The sol-gel method has the advantage of a low

processing temperature. Colloidal dispersions of metal oxide nanoparticles are created using this method [34, 35].

1.3.2. Top-Down approach:

a) Laser ablation:

Laser ablation is the process of removing and vaporising material from a solid surface using high-energy nanosecond laser light pulses to create nanomaterials [36]. To form the desired nanomaterial, we inject the ionised particles into a plume and then combine [37]. Thenwe deposit the resulting particles from the plume onto a substrate [38].

b) Mechanical alloying:

The Mechanical alloying (MA) process is a solid-state, powder particle producing technique in which it uses a ball mill [39] and/or rod mill [40] where the powder mixture placed in the ball mill is subjected to high-energy collisions from the balls, and the reactive process usually takes place in an inert atmosphere. This technique has two key processes: “repeated welding” and “fracturing of powder mixture”. Only if the rate of welding equals the rate of fracturing, and the average particle size of the powders remains relatively coarse, can the alloying process be continued [41]. Although, in general, mechanical alloying raw materials should include at least one ductile metal to act as a host or binder to hold the other ingredients together [42].

1.4. Mechanical alloying process:

1.4.1. The story behind the MA techniques:

The MA technique was the result of research conducted by John Benjamin and his colleagues at the Paul D. Merica Research Laboratory of the International Nickel Company (INCO) in the 1960s. This research was originally to produce a nickel-base superalloy, for gas turbine applications. It involved injecting nickel-coated graphite particles into a molten bath by argon sparging. The required corrosion and oxidation resistance was also included in the alloy by suitable alloying additions [39, 43]. E. C. Macqueen introduced the term “Mechanical alloying” in the late 1960’s in a US patent owned by INCO.In 1970, Benjamin pioneered the use of ball milling to produce complex oxide dispersion-strengthened (ODS) alloys for high-temperature structural applications such as jet engine parts [44].In 1983, Koch et al. [45] published the first novel technique for forming Ni_{60} Nb_{40} amorphous alloys from elemental Ni and Nb powders using high-energy ball milling. Since then, this method has successfully created a large number of alloys (figure 1.5).

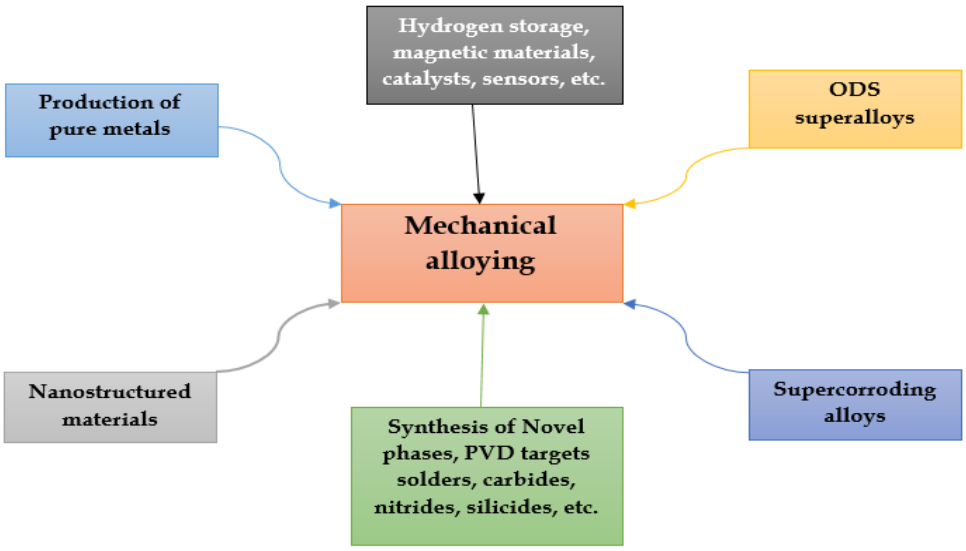

Figure 1.5. Application field of mechanical alloying

1.4.2. Steps of mechanical alloying:

The repeated welding, fracturing, and re-welding of a mixture of powders of the diffusion couples, as previously mentioned (figure 1.6), is the key process that takes place in a mill during the MA method to produce quality powder with regulated microstructure. In order to mechanically alloy successfully, you have to create a balance between fracturing and cold welding. Gilman and Benjamin [41] suggest two techniques to minimise cold welding and facilitate fracturing. The first method involves adding a processing control agent (PCA) to the deforming particles' surface (wet milling), which prevents the clean metal-to-metal contact needed for cold welding. The second method is to change the deformation mode of the powder particles so that they fracture and can deform to the broad compressive strains required for flattening and cold welding. Cooling the mill chamber is a technique for hastening fracture and establishing steady-state processing (effect of milling temperature) [46].

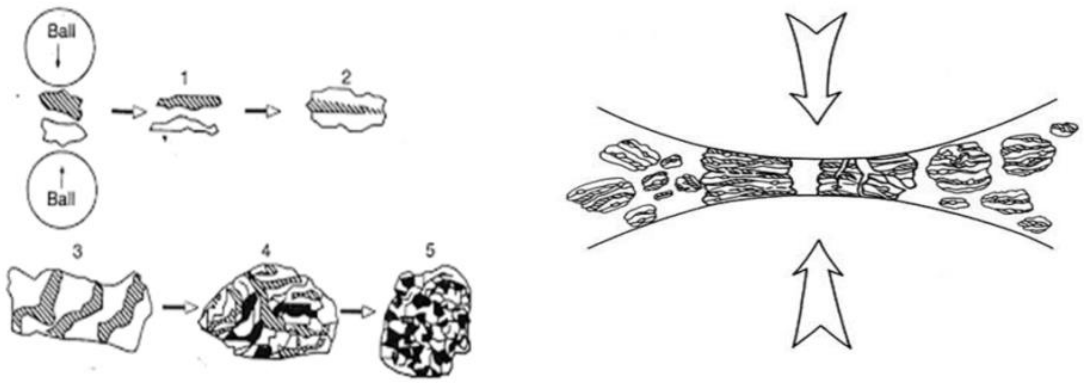

Figure 1.6. Step of mechanical alloying process

1.4.3. Type of milling:

Various types of high-energy milling equipment are used. They vary in size, milling efficiency, and additional cooling and heating arrangements.

a) High-Energy Ball Mills. Attritor or Attrition Ball Mill:

In 1922, Szigvari developed this mill for the industry in order to create fine sulphur dispersion quickly for use in rubber vulcanisation (figure 1.7), [41]. Most workers prefer the Szigvariattritorto other ball mills due to its operational flexibility. It consists of a water-cooled stationary vessel with a vertical shaft in the centre and impellers radiating from it. The shaft is connected to a geared, high-speed motor. Arms or 'lifters' stir the balls as the shaft rotates, causing them to lift up and fall back. As a result, there is a difference in movement between the balls and the matrices being milled, resulting in a much higher degree of surface contact.

At Japan's Defense Academy, Kimura and his colleagues [47] developed an attritor ball mill with a higher rotation speed of about 500rpm. They also outfitted the mill with a number of devices to control and measure the applied torque during the MA process. They proposed using this milling tool to create several amorphous alloy powders.

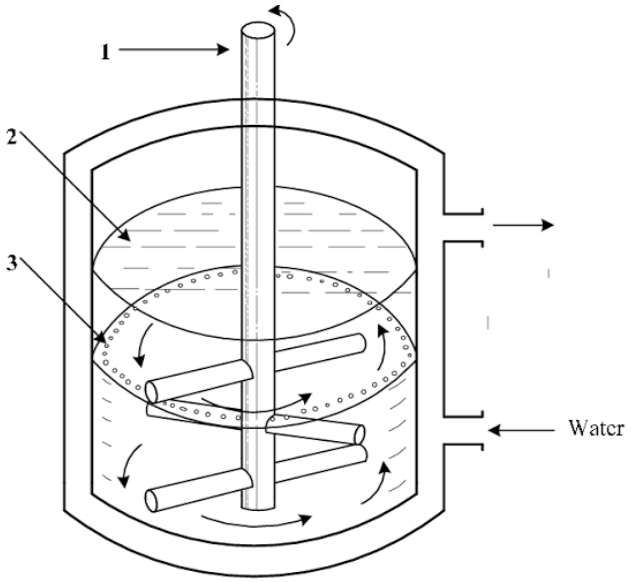

Figure 1.7. Schematic representation of attritor milling technique; 1- Shaft of the stirrer, 2- grinded material, 3- milling bodies.

b) SPEX vibratory mill:

Kuhn has been a strong proponent of the use of vibratory ball mills for MA. A vibratory ball mill is a long, closed tube that contains milling balls and powder [48, 49]. The charge of the powder and milling tools is agitated in three perpendicular directions at very high speeds,

up to 1200 rpm in this mill [50]. Moreover, it has a high amplitude (about 5 cm). As a result, the ball velocities are high (about 5m/s) and the impact force is unusually high. Laboratory research and alloy screening employs SPEX mills, which can mill 10-20 g of powder at a time. The most common type of mill has one vial containing the sample and milling balls, which is secured in the clamp and swung back and forth several thousand times per minute (figure 1.8)[51].

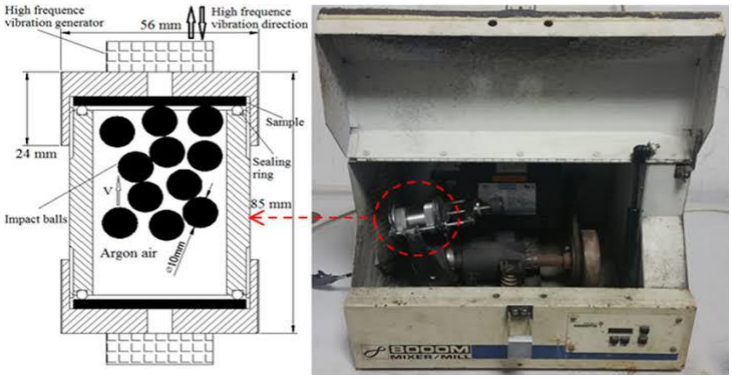

Figure 1.8. Schematic view of SPEX mill

c) Planetary ball mills:

The planetary ball mill (also known as the Pulverisette) is another common mill for MA experiments because it can mill a few hundred grammes of powder at a time. The planetary ball mill gets its name from the vial's planet-like movement (figure 1.9). Since the milling, stock and ball fall off the inner wall of the vial and the powerful centrifugal force reaches up to twenty times the gravitational acceleration in this form of mill [52].

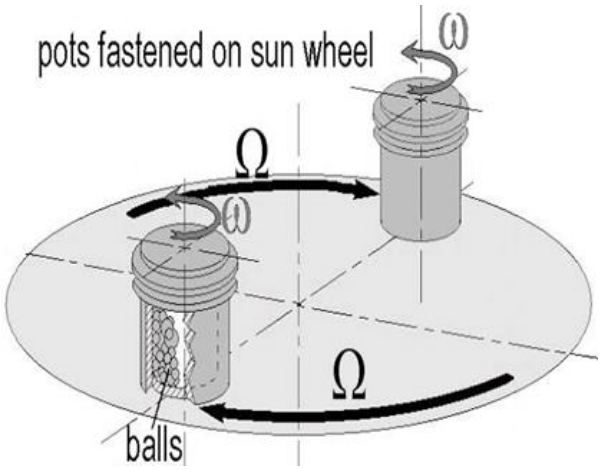

Figure 1.9. Principle of the planetary ball mill

Centrifugal forces created by the rotation of the supporting disc and the autonomous rotating of the vial affect the milling charge (balls and powders). Because the turning directions of the supporting disc and the vial are opposite, the centrifugal force alternately

synchronise. As a result, the milling media and charged powders alternately roll on the vial's inner wall and are raised and tossed into the bowl at high speeds (360 rpm) [53].

1.4.4. Factors affecting mechanical alloying:

Mechanical alloying is a difficult process that requires the optimization of numerous variables in order to achieve the desired product step and/or microstructure. The following are some of the most critical parameters that influence the powder's final composition [53]:

- Type of mill,
- Shape of the milling vials
- Milling speed
- Milling time
- Milling environment
- Milling atmosphere
- Milling ball-to-powder weight ratio
- Milling temperature
- Milling time
- The materials of the milling tools
- Type of milling media

1.4.5. Mechanism of alloying:

The employment of the MA method is for the three forms of processing described below:

a) Alloying:

To understand MA's mechanism, it is helpful to break the powder charge into three structures.

- **Ductile-Ductile system:** This is the perfect material combination for MA. In order to achieve alloying, Benjamin proposed that at least 15% of the ductile part be present. This was due to the fact that true alloying occurs as a result of repeated cold welding and fracturing of powder particles; cold welding cannot take place if the particles are not ductile [39].
- **Ductile-Brittle system:** Since the brittle oxide particles are scattered in the ductile matrix, typical ODS alloys fall into this group. Benjamin and others have identified the microstructural evolution in this type of system [44, 41]. In the ductile-brittle systems, MA normally results in a fine, homogenous dispersion of the brittle phase in the ductile matrix ductile-brittle system [54, 55].

- **Brittle-Brittle system:** It would seem that alloying is unlikely to occur in a device with two or more brittle components from a logical standpoint. This is because the lack of a ductile part prevents any welding from taking place, and alloying is not supposed to take place without it. Alloying in brittle-brittle component systems such as Si-Ge and Mn-Bi, on the other hand has been documented [56]. Milling of mixtures of brittle intermetallics also produced amorphous phases [57].

b) Metastable phase formation:

- **Amorphisation:** When White [58] milled an elemental mixture of Nb and Sn powders in 1976, he proposed a different method for synthesising amorphous materials at temperatures below the crystallisation temperatures. Koch et al. [46] were the first to develop this method, which they called mechanical alloying**.**
- **Nanocrystalline:** Several methods, such as inert gas condensation [59], rapid solidification [60], electrode location [61], sputtering, crystallisation of amorphous phases, and chemical processing [62], can be used to successfully synthesise nanocrystalline materials. As compared to amorphous phases, composites of amorphous and nanocrystalline phases have special properties, according to research [63]. Because of its simplicity, relatively inexpensive equipment, and ability to produce large quantities that can be scaled up to several tonnes [64], the mechanical alloying method has been considered the most effective tool for nanostructured materials among the various preparation options [65]. The extreme cold working on the ball-milled powders is responsible for the creation of nanocrystalline materials during MA of ceramics or metallic powders. This results in a significant increase in the number of flaws, which reduces the thermodynamic stability of the starting materials [63, 66].
- **Solid Solubility Extension (SSE):** Many beneficial properties of solid solution alloys include increased strength and elastic modulus, density improvements, and the removal of undesirable coarse second phases. The uniform precipitation of fine second-phase particles in a metallic matrix increases the strength and hardness of precipitation-hardening alloys [63].

c) Activation of solid state chemical reaction:

The formation of one or more product phases between the reactants is common in solid-state reactions, and the reaction volume decreases as the reactants become spatially separated. Initial contact areas, and therefore particle size, affect reaction rates as the reactant species

diffuse through the product phases. On reaction kinetics, factors that affect diffusion rates, such as defect structures and densities, local temperatures, and product morphology, play a significant role. By dynamically retaining high reaction interface areas [64] while simultaneously providing the conditions for rapid diffusion, mechanical alloying dramatically improves solid-state reaction rates [65].

1.5 Research work on Fe-Cu-Ni:

In 2021, Xuan Li et al. [66] published a report on "the topologically close packed $Fe_{70}Cu_{15}Ni_{15}$", in which they utilised molecular dynamics simulation to investigate nanoparticle of the alloy generated by rapid cooling from nanodroplet containing 1000 to 3000 atoms at a cooling rate of 0.01 k/p.s. The structures of nanoparticles of different size are examined in terms of the potential energy, the pair distribution function (PDF), and the largest standard clusters analysis. As a result, they discovered that: all the obtained nanoparticles have a core-shell structure with Cu atoms on the surface. The inside of the particle is either BCC crystalline, α phase crystalline or amorphous in structure. A topologically close-packed (TCP) nanoparticle is detected for the first time, in addition to the conventional body centred cubic (BCC) configuration. The increase in nanodroplet provokes an increase in crystallisation temperature and a decrease in the potential energy of the nanoparticles at 300K. For BCC nanoparticles, crystallinity increases with nanoparticle size, but this is not the case for TCP nanoparticles. These findings indicate a simple and efficient way to produce core-shell nanoparticles.

Jingjing Li et al. [67] performed a molecular dynamics MD simulation of Fe-Cu-Ni alloys. The evolution of structural features (such as coordination number CN, common neighbour sub-cluster CNS, largest standard LSC cluster and structural entropy S_{str}), indicated that the alloys are converted to glass, and that T_g increases when Ni is added. Depending on structural factors, the effect of Ni addition on the liquid state is either opposite or equal to that of the solid state. A study of the inverse effect revealed a new critical temperature (where crystal structures stop growing). The S_{str} is a useful tool for determining the degree of disorder in a system. The implications of these findings for the characteristics of disordered systems are enormous.

Eurotungstène et al. [7] produces metal powders used as a binder for diamond tools used for cutting abrasive materials. The metals used in the binder must provide a good compromise

between cutting speed and tool life. For almost 20 years, Eurotungstène has been producing Fe-Cu-Co alloy powders that fully met the technical specifications, except that since the implementation of the REACH system and the ban on the use of certain chemical elements such as cobalt for health reasons, the company has begun researching the Fe-Cu-Ni alloy to replace the alloy. Indeed, this combination is the first of its kind and can be a good compromise: Copper allows good sinterability of the powders; associated with nickel, it improves the hardness of the iron-based alloy. The sinterability of the powder should be further improved by the use of a fine powder from an innovative process developed by the company Eurotungstène.

To investigate the microchemical evolution caused by vacancy diffusion in Fe-Cu and FeCuNi alloys, N. Castinet.al [8] use a new atomistic kinetic Monte Carlo model that integrates local chemistry and relaxation effects when analysing the migration energy barriers of point defects. Cu precipitation, aided by the presence of Ni, is one of the primary causes of hardening and embrittlement in reactor pressure vessel steels used in existing nuclear power plants. Therefore these alloys are important for nuclear applications.

Qiongyu Zhou et al. [68] published a research paper on “electrochemical studies on passivation behaviour of Cu-Ni-Fe alloy in borate buffer solution at pH 8.4” in 2012. They used the method of copper oxide nickel oxide mixed powder applied on the surface of a mild steel sample and then treated under high temperature and hydrogen gas atmosphere to create a Cu-Ni-Fe alloy layer. The semiconductor properties of the passive films produced on the surface of the Cu-Ni-Fe alloy layer in borate buffer solution at pH 8.4 were investigated using the polarisation technique and Mott-Schattky analysis in conjunction with the point defect model. The passive film created on the surface was more compact, highly protective, and had a greater heating temperature. The carrier density and vacancy diffusion coefficient of the passive film produced on Cu-Ni-Fe alloys were reduced. In a borate buffer solution at pH, the vacancies diffusition is approximately 10^{-20} m^2s^{-1}.

CHAPTER 2: ELABORATION CHARACTERISATION TECHNIQUES

2. Elaboration and characterisation techniques

2.1. Introduction:

This chapter illustrates the experimental methods used. It is divided into two parts: the first part is devoted to the structural studies of the elemental powders used in the elaboration of our alloy. The second part deals with the elaboration techniques and characterisation of the morphological, structural and magnetic properties. The mechanical alloying of the Fe-Cu-Ni alloy was carried out for a 10hours of milling. The kinetics of the formation of the considered alloy and the evolution of the lattice parameter during the milling were studied by means of X-ray diffraction. The evolution of the magnetic properties as a function of the milling time was studied using a vibrating sample magnetometer VSM.

2.2. Properties of the Fe-Cu-Ni powder alloy:

The alloy we are going to use in this project is based on three elements: Fe, Cu, and Ni. Their combination is totally new in this domain, but why did we specifically use these three elements? Table 2.1 shows the different properties of the iron, copper, and nickel.

Table 2.1.Physical properties of iron, copper and nickel

	Fe	**Cu**	**Ni**
Atomic Number (z)	26	29	28
Electronic configuration	[Ar] $3d^6 4s^2$	[Ar] 3d 10 4s 1	[Ar] $3d^8 4s^2$
Metal radius (A°)	1.27	1.28	1.24
thermal expansion 20°C (10^{-6}/°C)	12	17	13
Magnetic state	Ferromagnetic (α-Fe); Anti-ferromagnetic (γ-Fe)	Diamagnetic	Ferromagnetic
Density at 20°C ($g.cm^{-3}$)	7.8	8.9	8.9
Melting point (°C)	1536	1083	1453
Ionic radius	0.076 nm (+2) ; 0.064 nm (+3)	0.096 nm (+1) ; 0.069 nm (+3)	0.069 nm (+2) ; 0.06 nm (+3)
Standard potential (V)	- o.44 V (Fe^{2+}/ Fe) ; 0.77 V (Fe^{3+}/ Fe^{2+})	+ 0.522 V (Cu^{+}/ Cu) ; + 0.345 V (Cu^{2+}/ Cu)	- 0.25
Young's modulus	196	124	214

Copper is known as the most noble of the metals in common use; it has excellent resistance to corrosion in the atmosphere and the fresh water. While, the iron is an excellent ferromagnetic material, Ni is a hard metal with magnetic properties similar to the Fe [69]. According to a preliminary study of Fe-Cu-Ni alloys combined as a good compromise, copper has good sinterability when combined with nickel, and it increases the hardness of the iron-based alloy. The use of a fine powder from an innovative process should increase the powder's sinterability even more [70, 71]. The addition of Ni (a third-party element) to FeCu alloy allows speeding up the nucleation rate and enhancing the density of Cu particles [72,73].

2.2.1. Iron properties:

Iron can exist in two crystalline forms (Figure 2.1). The stable form under ordinary conditions of temperature and pressure is the body cantered cubic (BCC) form of α-iron. Between 910°C and 1390°C, the face-centred cubic form of γ-iron is observed. Above 1390°C and up to the melting point, the body cantered cubic structure of δ-iron is found. This results in two points of allotropic transformation (Table 2.2).

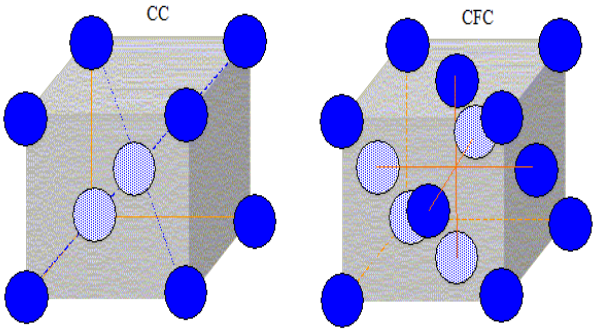

Figure 2.1.Crystallographic structure of Iron

Table 2.2.Theoretical density of the allotropic varieties of iron α and iron γ.

	α-iron	**γ-iron**
number of atoms in a lattice	2	4
Side of the unit cube	a=287 pm = 2.87 10^{-10} m	a=347 pm = 3.47 10^{-10}m
Volume of the cube	a3 = 2.36 10^{-29} m3	a3 = 4.18 10^{-29} m3
Mass of atoms in a lattice	m=2M/NA= 2*55.85 10^{-3} / 6.02 1023 =1.855 10^{-25} kg	m=4M/NA= 4*55.85 10^{-3} / 6.02 1023 =3.71 10^{-25} kg
Density m/ a3 (kg m-3)	7849	8879

2.2.2. Nickel properties:

Nickel crystallises in a face-centred cubic structure FCC as shown in Figure 2.2; its properties are shown in table 2.3.It promotes the formation of an austenitic solid solution. Iron and nickel belong to the group of 3d transition elements.Therefore these pure elements and

their alloys also exhibit properties of this group, which are characterised by the incomplete 3d electronic layer and the complete 4s electronic layer. [74].

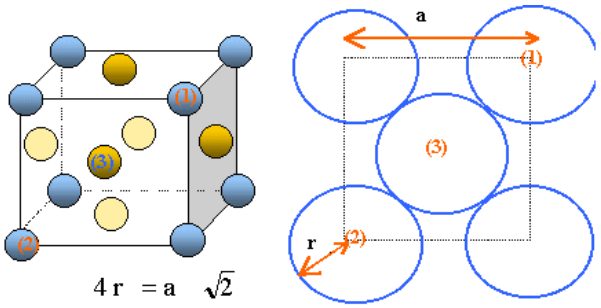

Figure 2.2.Crystallographic structure of Nickel

Table 2.3. Crystallographic properties of Nickel.

	Nickel
Number of atoms in a mesh	4
Side of the unit cube	a= 3.53 10^{-10} m = 353 pm
Volume of the cube	a3 = 4.39 10^{-29} m3
Mass of atoms in a lattice	m =4 M (Ni) / N_A = 4 *58.7 10^{-3} / 6.02 10^{23} = 3.90 10^{-25} kg.
Density m/ a3 (kg.m^{-3})	8.90 10^3

2.2.3. Copper properties:

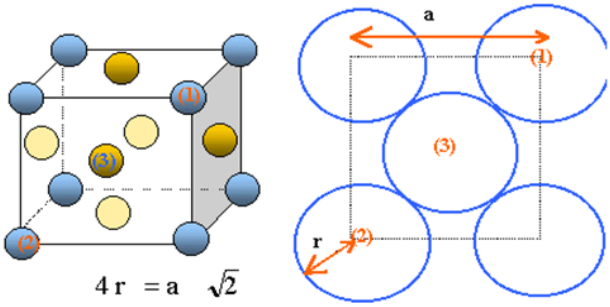

Figure 2.3.Crystallographic structure of Copper

Table 2.4.Crystallographic properties of the Copper

	Copper
Number of atoms in a mesh	4
Side of the unit cube	a= 3.60 10^{-10}m=360pm
Volume of the cube	a^3 =4.6656 10^{-29} m^3
Mass of atoms in a lattice	4 M (Cu) / NA =4.219 10^{-25} kg.
Density m/ a3 (kg m-3)	8.85 103

2.2.4. Binary system Fe-Ni:

a) Phase diagram:

The phase diagram is an essential tool in metallurgy when developing new alloy compositions. It allows determining the domains of existence of the phases that can be

encountered in the selected system and is essential for interpreting the microstructures and understanding their genesis [75].

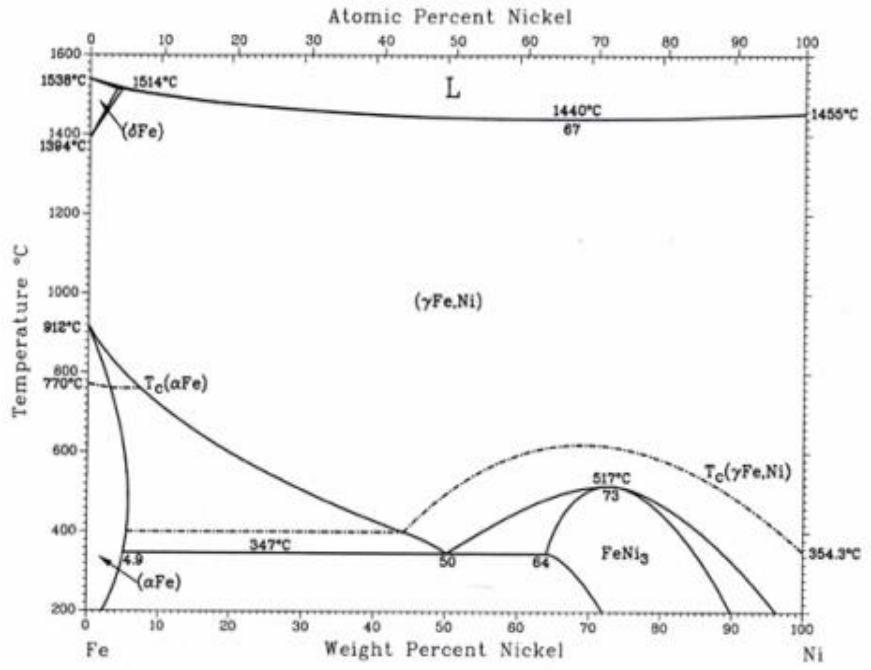

Figure 2.4.Phase diagram of the Fe-Ni system [75]

Figure 2.4 shows the phase diagram of the FeNi system; this diagram shows the following different phases: the alpha α phase (CC), the phase δ (FCC), the paramagnetic phase when the % of Ni is weak, γFeNi phase. The solution solid γFeNi extends over the entire compositional range at high temperatures and forms a very narrow two-phase domain with the liquid, with a minimum at 1443°C for 66 % Ni. The solid solution BCC δFe occupies a reduced compositional range with a maximum solubility of at3.5% Ni at 1514°C and forms a peritectic equilibrium with the liquid and the FCC γ solid solution at 1514°C. Below 912°C, the solid solutions γFe and αFe form a two-phase domain with a retrograde solubility of Ni in αFe (maximum solubility of 6 at.% Ni maximum at 500°C) [75].

b) Curie temperature:

Figure 2.5 shows the variation of the Curie temperature for the iron-rich compositions as the amount of nickel increases. Mossbauer transmission tests down to liquid-nitrogen temperature were used to estimate the ferromagnetic-transition temperature Tc of thoroughly homogenised Ni-Fe alloys. For Ni contents ranging from 24% to 35 %(atomic). The findings reveal that Tc reduces rapidly as the Ni concentration falls, following a nonlinear pattern that differs from the linear pattern seen in other Ni compounds. The current findings are consistent with those of other writers. However, they differ slightly. From other sourcess, most likely from less homogeneous samples [76].

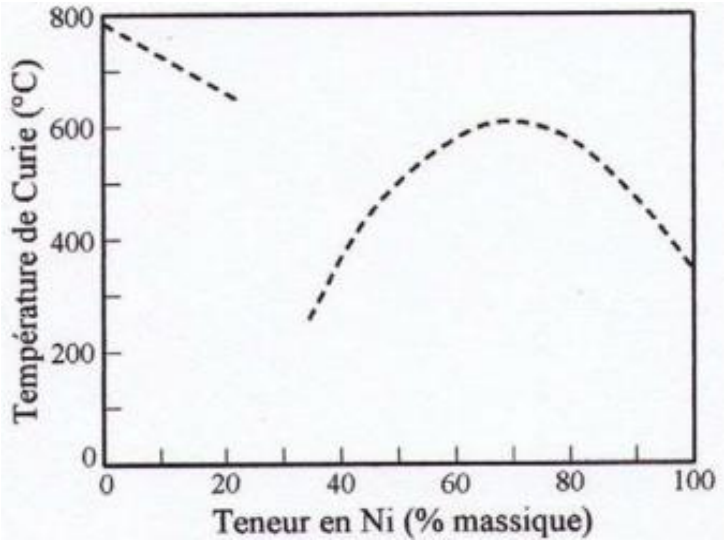

Figure 2.5.Evolution of Curie temperature for the iron-rich compositions as the amount of Nickel increases [77]

c) Application of the alloy Fe-Ni:

The table 2.5 summarises the applications of Fe-Ni

Table2.5. Application of the alloy FeNi [74]

Domain	Type of Fe-Ni	Properties of the alloy
Watchmaking	The stator of the stepper motor is made of 80% Nickel alloy	Excellent cutability Low coercivity field High saturation Induction
Electromagnetic Shielding	Mumetal and supra50 for shielding in composite form. Sandwich sheets combining Fe-Ni alloys.	High magnetic permeability
Automotive field	Fe-50%Ni alloy for torque transducers for accurate wheel positioning	High saturation induction
	Refractory alloys for cylinder head gaskets	Oxidation and high temperature resistance
	Maraging alloys (FeNiMbCo special steels) For variable transmission belts	Yield strength up to 2000 Mpa with very high fatigue resistance
	Fe-36%Nickel Invar for automotive injection	Dilatation

2.2.5. Binary system Fe-Cu:

a) Phase diagram:

Swartzendruber has proposed a synthesis of the Fe-Cu system. The phase diagram of this system (Figure 2.6) is characterised by a broad two-phase domain that extends from the Fe-rich α- body centred cubic solid solution (BCC) to the face-centred cubic (FCC) solid solution. [75]

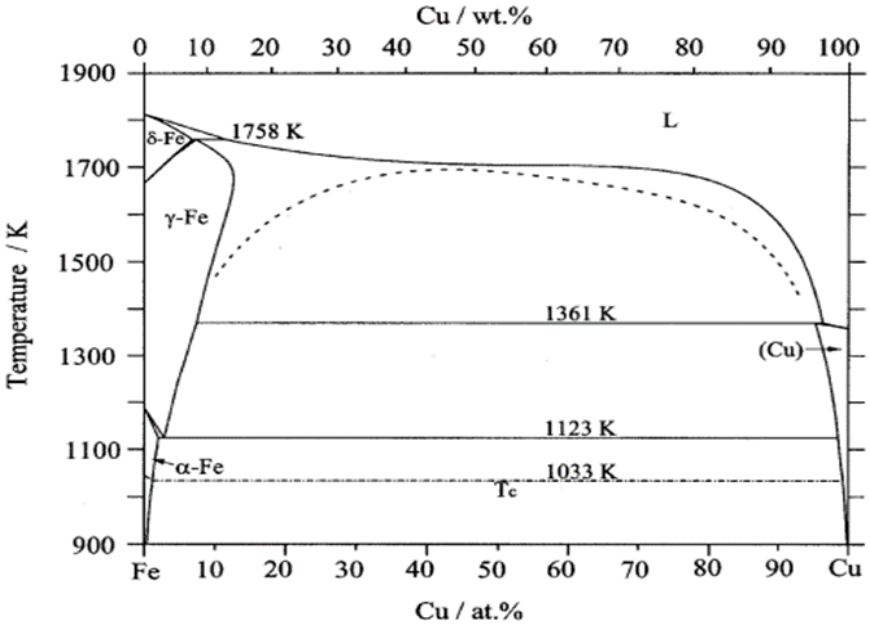

Figure 2.6.The phase diagram of the system FeCu [75]

2.3. Elaboration technique:

2.3.1. Elaboration condition:

For the elaboration of nano-structured powders based on iron, copper, and nickel, we have used a planetary ball mill PM400 at Blida surface treatment and mechanical materials laboratory (figure 2.7).

Figure 2.7.Planetary mill PM400

The device used contains two WC jars. The milling speed was set at 350 rpm for a cycle of 15 minutes of running followed by 15 minutes of rest in order to avoid rise of the temperature inside the jars.

2.4. Characterisation technique:

2.4.1. Scanning electron microscope:

a) Definition:

The scanning electron microscope (SEM) is a device that produces magnified images that reveal microscopic-scale information about a specimen's size, shape, composition, crystallography, and other physical and chemical properties [78]. This type of microscope is the most common used microscope. It examines microscope structure by scanning the surface of materials in the same way that scanning confocal microscopes do, but with much higher resolution and depth of field. A focused electron beam scans over the surface area of a specimen to create a SEM image. Because of its large depth of field, the 3D appearance of a SEM's images is perhaps its most important feature. SEM is a system that allows us to extract chemical information from a specimen using a variety of techniques, including the X-ray energy-dispersive spectrometer (EDS) [79].

b) History:

The origins of electron microscopy can be traced back to the development of electron optics. Knoll and Ruska attempted to estimate the resolution limit of an electron microscope limit of an electron microscope in 1932. Assuming that the light microscope's resolution limit formula was still valid for material waved, they replaced the light wavelength with the electron wavelength at a 75 kV accelerating voltage. Ruska and Knoll experimented with implementing Busch's lens formula. Their efforts resulted in the creation of the first transmission electron microscope (TEM) with a magnification of 16 in 1931 [80]. Zworykin described and developed the first true SEM in 1942 [81].

c) Image formation in SEM:

The electron column, the specimen chamber, and the computer/electric controls are three major sections of the SEM instrument. The topmost section of the electron column is made up of an electron gun that produces an electron beam. The beam is focused into a small diameter (few nanometres) probe by electromagnetic lenses located within the column. The scan coils in the column raster the probe across the surface of the sample in the chamber at the end of the column. To allow electron beam generation and advancement, the gun, the column, and specimen chamber are kept under vacuum. The beam's electrons penetrate a few microns into a bulk sample's surface, interact with its atoms, and generate a variety of signals, including secondary and backscattered electrons, as well as characteristic X-Rays, which are collected and processed to obtain images and chemistry of the specimen surface (figure2.8).

In the SEM, the diameter of the electron probe corresponds to the image's ultimate lateral resolution [82].

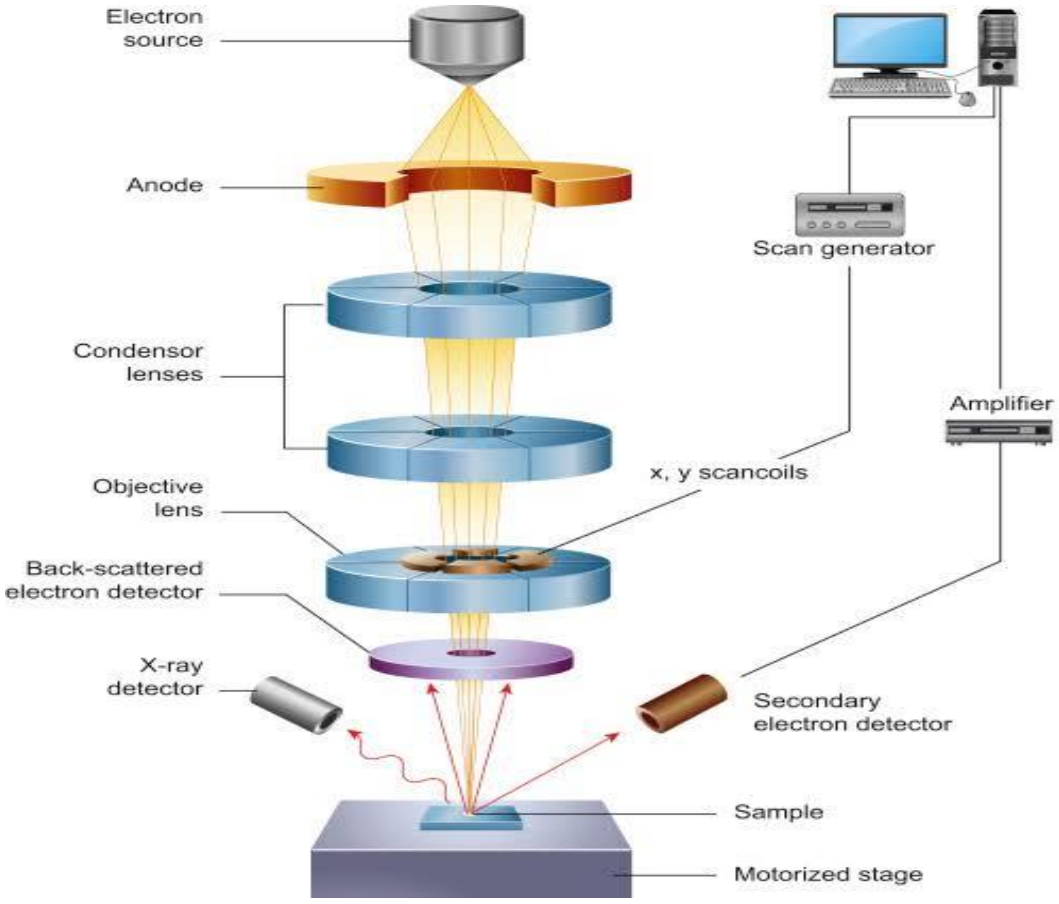

Figure 2.8.Schematic diagram of the core components of an SEM microscope

- **Backscattered electrons:** Beam electrons are subjected to multiple elastic and inelastic scattering events, resulting in a large region within the specimen known as the interaction volume. The magnitude of each type of scattering is determined by the beam energy, the atomic number of the target, and the angle of tilt used. Backscattering occurs when electrons in an elastically scattered beam are deflected through large angles (>90) and eventually find their way out of the specimen. Backscattered electrons (BSE) are electrons that were originally part of the incident electron beam that struck the surface of the specimen. The majority of the electron signal emitted by the specimen is made up of backscattered electron. These electrons account for a sizable portion of the incident beam's total energy [83].
- **Secondary electron:** In addition to BSE, electrons from the target material are ejected from the specimen. These electrons are typically loosely bound outer shell electrons that reside close to the specimen surface and are struck elastically by the incident beam's

electrons. Secondary electrons are electrons that originate in the specimen material and are ejected from the specimen (SE). A detector can collect these and combine them to form a secondary electron image. The contrast exhibited by SE is known as topographic contrast [83].

- **X-Rays:** The primary electron beam enters the specimen material and interacts with the atom's inner shells. As a result, the target atom's inner-shell electrons are ejected from their orbits and leave the atom's boundaries. The process of electron ejection creates an orbital vacancy, converting the atom into an excited or energized iron. This vacancy is immediately filled when an electron from the outer shell is transferred to the inner shell, bringing the atom to its ground (lowest energy) state and releasing energy equal to the difference in the binding energies of the two shells [84].

d) General sample preparation:

Sample preparation consists of four steps: a) fixation, b) dehydration, c) critical point drying, and d) coating. All four steps can differ significantly and may need to be modified for specific applications. Adequate sample preparation is critical for preserving structural integrity and obtaining accurate information on cellular components and molecular composition [85].

e) Equipment:

The figure 2.9 depicts Gemini SEM 300 microscopy of CRTI used in our work, with a 30Kv acceleration voltage and a distance of 15 mm, equipped with an X-ray dispersive energy spectrometer. The samples that were tested were placed on aluminium supports.

Figure 2.9.Photograph of SEM device equipped with EDS

2.4.2. Energy dispersive X-Ray spectroscopy:

a) Definition

Energy-dispersive X-ray spectroscopy (EDS) is a powerful yet simple technique for determining which elements and thus chemical compounds are present in a specific specimen. After bombarding a sample with high-energy electrons in an electron microscope, EDS detects the characteristic X-rays produced by each element. Using a technique known as X-ray mapping, information about a sample's elemental composition can then be overlaid on top of a magnified image of the sample [86]. In 1995, John Friel and his team at Princeton Gamma-Tech in the United States, now part of thermo Fisher Scientific, developed a method known as position-tagged spectrometry (PTS). This method has the significant advantage of allowing an entire spectrum to be stored at each pixel in the scanned image. The X-ray detectors that are commonly used today differ only in detail from those used in the early 1970s. However, it is because of the details, such as greatly improved resolution, sensitivity to soft X-rays, predictability of characteristics, and collection efficiency, that EDS analysis in the electron microscope has become an indispensable tool in such a wide range of applications, from manufacturing settings to cutting-edge research laboratories [87,88].

b) Principle of energy dispersive X-Ray spectroscopy:

EDS spectroscopy is used to determine the elemental composition of a substance using a scanning electron microscope. Elements with atomic numbers greater than boron can be detected by EDS at concentrations of at least 0.1 percent. Material evaluation and identification, contamination identification, spot detection analysis of regions up to 10 cm in diameter, quality control screening, and other applications are all possible with EDS [89].

c) Equipment:

- **Electron beam source:** Because EDS is used in conjunction with a scanning electron microscope, the same electron gun (Field Emission) is used as the incident electron source, and lenses and apertures are used to focus the beam.
- **X−ray Detector:** The EDS detector measures the X-ray counts versus X-ray energies. As X−rays strike the surface of the detector, a charge pulse is created. This charge pulse is directly proportional to the energy of the incident X−ray.
- **Pulse Processor:**A charge sensitive preamplifier is employed to convert the charge pulse to a voltage pulse.

- **Analyser:**A multi-channel analyser is used to sort pulses by voltage in the signals, which are received by the analyser. The energy of the X-ray can be obtained by measuring the voltage of the charge pulses.

d) Accuracy of EDS:

EDS identifies the chemical elements present in a sample and estimates their relative abundance. EDS is also useful for measuring the thickness of multi-layer coatings on metallic coatings and analysing various alloys. Several factors influence the precision of this quantitative analysis of sample composition [90]:

- Many elements' X-ray emission peaks will overlap (for example, Ti Kβ, V Kα, Mn Kβ and Fe Kα).
- The nature of the sample also has an impact on the accuracy of the measured composition.
- X-rays are emitted in all directions, but not all of them may escape the sample.

2.4.3. X-Ray diffraction:

a) Definition:

For nanoscale materials, powder X-ray diffraction (XRD) is a common characterisation technique. Powder XRD analysis provides valuable information that complements various microscopic and spectroscopic methods, such as phase identification, sample purity, crystallite size, and, in some cases, morphology. The information provided by this bulk technique can be correlated with microscopy data to see if microscopic observations of a small number of particles are representative of the majority of the sample. However, despite its importance and widespread use, powder XRD data for nanoscale materials is not always completely utilized and it is sometimes misconstrued [91].

For well over a century, X-rays have been used for a variety of sensing, imaging, and detection tasks. Only a few months after Rontgen discovered the X-ray in 1895, radiography imaging was born, and X-ray diffraction (XRD) was already being used to aid in the determination of crystalline structure by 1912. Max Von Laue's pioneering work, as well as the father-son team of W.L and W.H. Bragg, provided both demonstrations and interpretations of the physics behind XRD, allowing for a variety of refinements, generalizations, and simplifications of the method. As a result, XRD is now a quantitative, versatile, and widely used tool in science and engineering [92].

b) Principle:

The wavelength and frequency of electromagnetic radiation (waves) produced by the diffractometer are determined by the source. Because X-rays are the only type of energy with the optimal wavelength for inter-atomic-scale diffraction, they are frequently used as the source. When these waves reach the sample, they either are reflected off the surface or enter the lattice, where the atoms diffract them.

According to Bragg's law (figure2.10), if the atoms are arranged symmetrically with a separation distance d, the waves will only interfere constructively where the path-length difference 2d sin is an integer multiple of the wavelength, resulting in the maximum of diffraction. These waves interfere destructively at points where the waves are out of phase between intersections, but do not cause bright spots in the diffraction pattern [93].

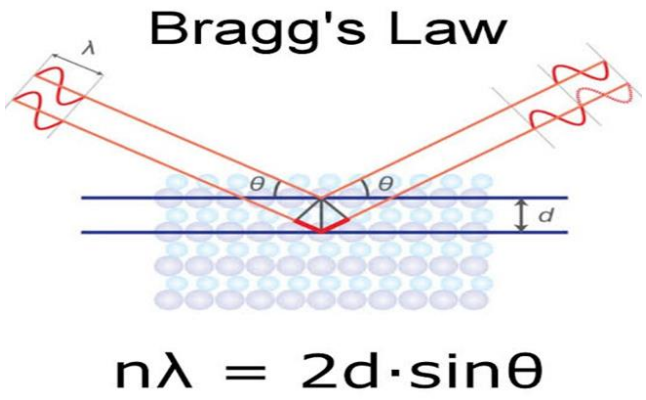

Figure 2.10.Bragg's Law Principle

c) Equipment:

Figure 2.11 shows the XPERT PRO diffractometer, which is used to perform X-ray diffraction analysis.

Figure 2.11.Photograph of the device used to perform XRD

All measurements are taken with an anticathode of Cobalt Co k (λ= 1.78901 A°; 40 kV, 30 mA). The acquisition of diffractogram data is between 10° < 2θ < 110°. The powders were dispersed on aluminium sample holders.

2.4.4. Vibrating sample magnetometer (VSM):

a) Definition:

Vibrating Samples Magnetometer instruments are used to determine the magnetic behaviour of a sample for a wide range of materials. The principle of operation of VSM is based on Faraday's law. VSM was invented in 1955 at MIT Lincoln Laboratory by Simon Foner, who published his findings in 1959 [94].

b) Process:

The most widely used instrument for measuring magnetization is the vibrating sample magnetometer. There have been numerous modifications and improvements to this instrument since its invention by S. Foner [94, 95]. The basic principle, however, remains the same and it is very straightforward. The magnetic specimen is vibrated with a vibrator at a specific frequency and amplitude in this technique. A static magnetic field is used to magnetise the sample at the same time. A set of pick-up coils is now placed near the magnetised sample in order to detect the signal voltage induced in the coils as a result of the change in magnetic flux caused by the magnetised sample's vibration (figure 2.12) [96].

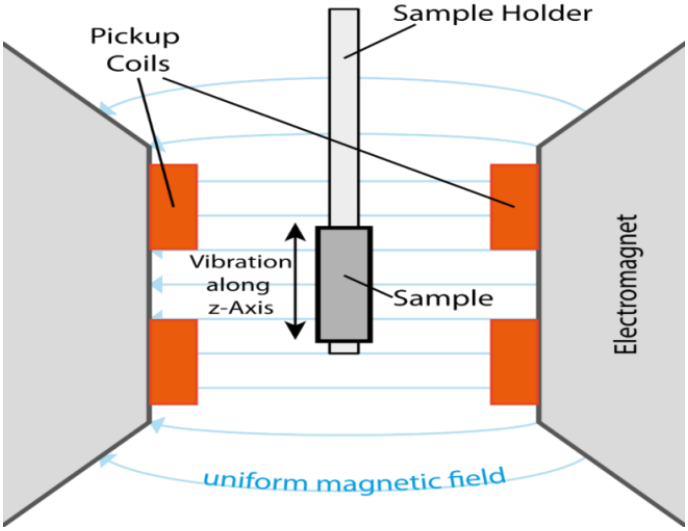

Figure 2.12.VSM schematic

c) Advantages and dis-advantages:

In comparison to other magnetometers, the precision and accuracy of VSMs can reach 10^{-6} emu [97]. As a result of the VSM's ability to test samples at a variety of different angles in relation to their magnetization, researchers can minimise the effects of external influences.

However, due to the sample's demagnetizing effects, VSM's are not suitable for determining the magnetization loop. In addition, VSM's are affected by the temperature of the sample and can not be used on delicate samples that cannot be accelerated (from the vibration) [97, 98].

d) Hysteresis loop:

A magnetic hysteresis, also known as a hysteresis loop, is a representation of a ferromagnetic materials magnetising force (H) versus magnetic flux density (B).

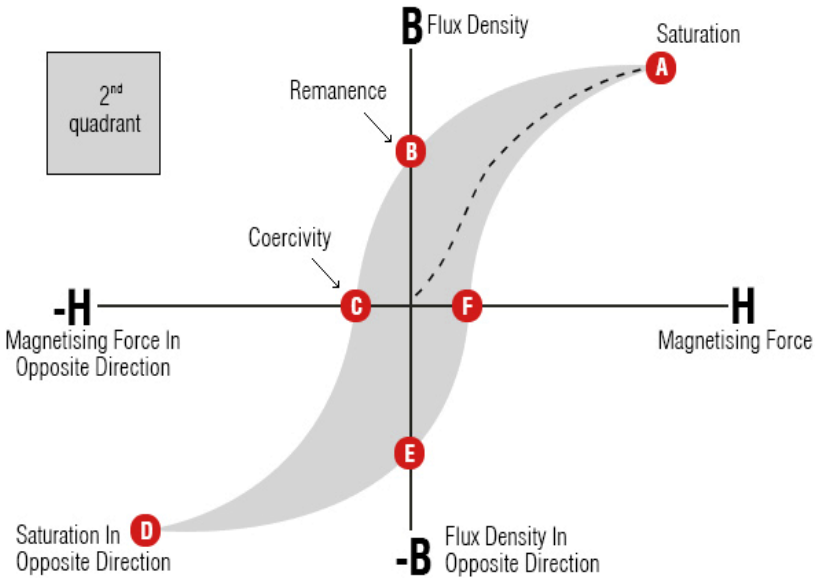

Figure 2.13.Hysteresis loop

The curvature of the hysteresis is specific to the material being studied and can vary in size and shape (i.e. narrow or wide) (figure 2.13).

e) Equipment:

The figure 2.14 shows a photograph of a vibrating sample magnetometer (VSM).

Figure 2.14.Vibrating Sample Magnetometer device

The magnetic behaviour of the different samples is studied by plotting hysteresis cycles, which characterise the variations in statistical magnetization as a function of the applied magnetic field M (H).

2.4.5. Classification of magnetics materials:

Magnetic materials are classified according to whether their magnetic dipoles are parallel, anti-parallel, or not at all. The material is said to be paramagnetic or diamagnetic if the individual dipole moments are randomly oriented so the $\sum m=0$. The materials are frequently referred to as non-magnetic in non-physical contexts. However, if an external magnetic field is applied, paramagnetic and diamagnetic materials can be partially oriented. The material is said to be ordered if the dipole moments are not randomly oriented despite the absence of an external magnetic field [99]. Ferromagnets, antiferromagnets, and ferrimagnets are three types of ordered magnetic materials.

a) Diamagnetism:

- Very weak; exists only in the presence of an external field; non-permanent.
- An applied external field acts on atoms of a material, slightly unbalancing their orbiting electrons, and creating small magnetic dipoles within atoms, which oppose the applied field. This action produces a negative magnetic effect known as diamagnetism.
- The induced magnetic moment is small, and the magnetization (M) direction is opposite to the direction of the applied field (H).
- Thus, the relative permeability is less than unity, i.e., magnetic susceptibility is negative, and is in order of -10^{-5}.
- Materials such as Cu, Ag, Si, Ag and alumina are diamagnetic at room temperature.

b) Paramagnetism:

- Slightly stronger; when an external field is applied, dipoles line-up with the field, resulting in a positive magnetization. However, the dipoles do not interact.
- Materials which exhibit a small positive magnetic susceptibility in the presence of a magnetic field are called para-magnetic, and the effect is termed para-magnetism.
- In the absence of an external field, the orientations of atomic magnetic moments are random, leading to no net magnetization.

- When an external field is applied, dipoles line-up with the field, resulting in a positive magnetization.
- However, because the dipoles do not interact, extremely large magnetic fields are required to align all of the dipoles.
- In addition, the effect is lost as soon as the magnetic field is removed.
- Since thermal agitation randomises the directions of the magnetic dipoles, an increase in temperature decreases the paramagnetic effect.
- Para-magnetism is produced in many materials, like aluminium, calcium, titanium, and alloys of copper.
- The magnetic susceptibility of these materials is slightly positive and lies within the range$+10^{-5} to +10^{-2}$.

c) Ferromagnetism:

- Both dia and para magnetic materials are considered non-magnetic because they exhibit magnetization only in the presence of an external field.
- Certain materials possess permanent magnetic moments even in the absence of an external field.
- This is the result of permanent unpaired dipoles formed from unfilled energy levels.
- These dipoles can easily line-up with the imposed magnetic field due to the exchange interaction or mutual reinforcement of the dipoles. These are characteristics of ferromagnetism.
- Materials with ferromagnetism (examples: Fe, Co, Ni, Gd) possess magnetic susceptibilities approaching 106.
- Above the Curie temperature, ferromagnetic materials behave as para-magnetic materials and their susceptibility is given by the Curie-Weiss law, defined as:$\chi_m = \frac{C}{T-T_C}$

Where C: material constant, T: temperature, Tc: Curie temperature.

- Ferro magnets are very strong; dipoles line up permanently upon application of an external field. It has two sub-classes:
  - **Anti-ferro-magnetism:**
- Dipoles line-up, but in opposite directions, resulting in zero magnetization.
- Ex: Mn, Cr, MnO, NiO, CoO, and $MnCl_2$.

- The exchange interaction, which is responsible for parallel alignment of spins, is extremely sensitive to inter-atomic spacing and to atomic positions. This sensitivity causes anti-parallel alignment of spins.
- When the strength of anti-parallel spin magnetic moments is equal, no net spin moment exists, and resulting susceptibilities are quite small.
- One noticeable characteristic of anti-ferro-magnets is they attain maximum susceptibility at a critical temperature called Neel temperature. At temperatures above this, anti-ferro-magnets become para-magnetic.

➢ **Ferrimagnetism**:

- Some ceramic materials exhibit net magnetization.
- Ex: Fe_3O_4, $NiFe_2O_4$, (Mn. Mg) Fe_2O_4, $PbFe_{12}O_19$, Ba $Fe_{12}O_{19}$, YIG – yttrium iron garnet $Y_3Fe_5O_{12}$.
- In a magnetic field, the dipoles of a cation may line up with the field, while the dipoles of other cations may not. These ceramics are called ferrites, and the effect is known as ferrimagnetism.
- Ferrimagnetism is similar to antiferro magnetism in that the spins of different atoms or ions line up anti-parallel. However, the spins do not cancel each other out, and a net spin moment exists.
- Below the Neel temperature, therefore, ferromagnetic materials behave very much like ferromagnetic materials and are paramagnetic above the Neel temperature.
- These materials exhibit a large but field dependent magnetic susceptibility similar to ferromagnets.
- They also show Curie-Weiss behaviour. As these ceramics are good insulators, electrical losses are minimal, and hence ferrites have a lot of applications in devices such as high-frequency transformers.

CHAPTER 3. RESULTS AND DISCUSSIONS

3. Results and discussion

3.1. Introduction:

This chapter is dedicated to the interpretation of the morphological, microstructural, and magnetic characterizations of Fe Cu Ni powder alloy obtained using the techniques of X-ray diffraction (XRD), scanning electron microscope (SEM), and vibrating sample magnetometer (VSM), respectively. For Fe, Ni, and Cu, the initial elemental powder particle sizes are 80 µm, 55 µm, and 60 µm, with purity of 99.5%, 99.9%, and 99.9%, respectively.

Tungsten carbide (WC) balls are used to mill the mixture of Fe, Cu, and Ni powders in a high-energy planetary ball mill PM 400 operating in an argon atmosphere for 10 h of milling with 350 rpm. Initially, the powder mixtures were composed of $Fe_{70}Cu_{30-x}Ni_x$, where x=0, 10, 15, 20, or 30. After milling, the powders were examined using a Gemini SEM 300 equipped with an EDS unit (Energy Dispersive X-ray Analyses) and a 30 kV accelerating voltage.

The morphology, size, and particle distribution of the milled powders were analysed using visual basic software and several SEM images, and scanning electron microscopy was used to characterise them. Co kα radiation was used by XPERT PRO to characterise the crystal's X-ray diffraction (XRD). A maximum applied field of 20 kOewas used in the Vibrating Sample Magnetometer to determine magnetic properties.

3.2. Structural characteristics of Fe-Cu-Ni:

3.2.1. X-ray diffraction pattern characteristics:

It is well known that the induction of crystal defects such as dislocations, grain boundary vacancies, and interstitials during mechanical alloying by deforming heavy plastics into powder particles promotes solid-state processes at room temperature. The structure of mechanically alloyed powders can vary depending on the initial mixture: grain refinements, solid solution diffusion, and/or the development of new phases [51].

Figure 3.1 depicts the XRD patterns of the pure Fe, Cu, and Ni powder. The graph shows the intensity of diffraction peaks as a function of Bragg angle. The results show the coexistence of the pure Fe, Cu, and Ni elements before the milling and it shows that they are in good crystalline conditions [100].

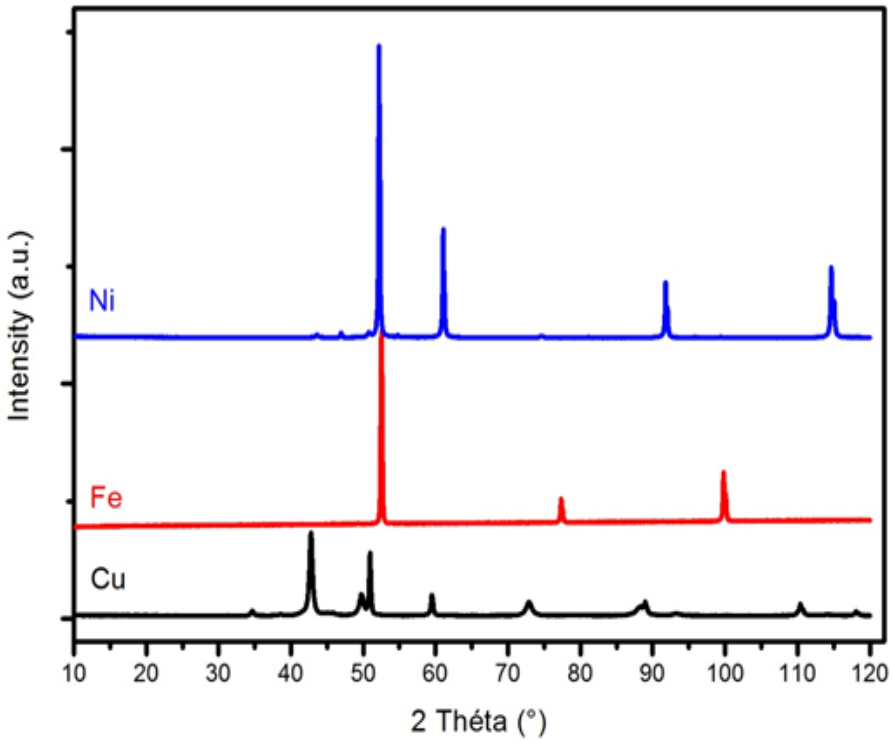

Figure 3.1.XRD patterns of pure Fe, Cu and Ni powder

The X-ray diffraction pattern for the $Fe_{70}Cu_{30-x}Ni_x$ (x=0.10.15.20.30) powder mixture is shown in figure 3.2.

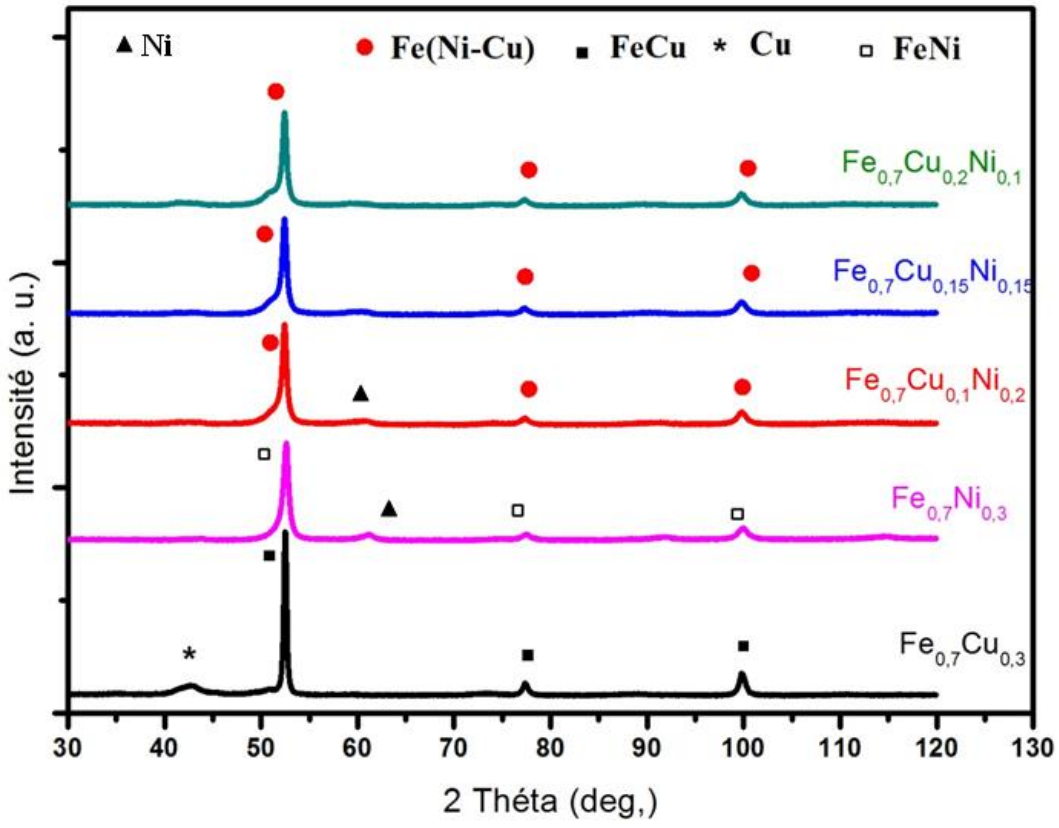

Figure 3.2 a. XRD patterns of Fe-Cu-Ni milled powder with different concentration

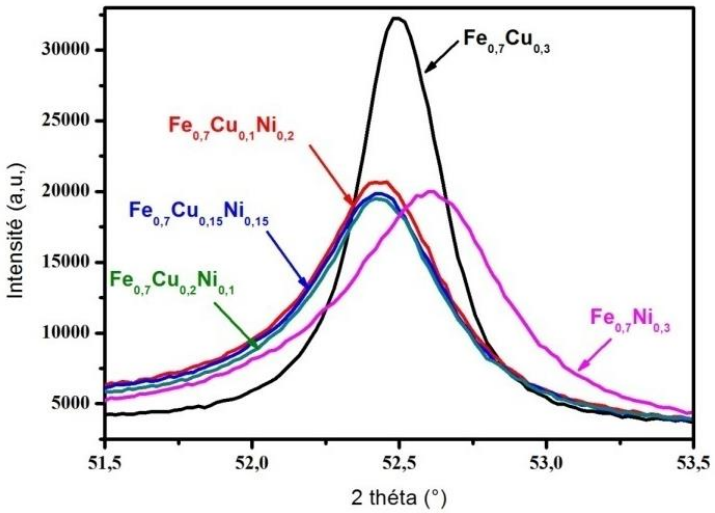

Figure 3.2 b. Zoom of XRD patterns of Fe-Cu-Ni milled powder with different concentration between 51.5° and 53.5° region

After 10 hours of MA, the peak relating to the copper phase becomes less intense and eventually disappears. This indicates that the grain size of copper powders is being refined at a faster rate [101]. Furthermore, the intensity of the iron phase peaks decreases, indicating that due to the almost identical atomic radius (Fe= 126pm, Cu=128pm),copper atoms are gradually being introduced into the iron structure [102]. For the Fe-Ni, the characteristics of Ni lines decrease in amplitude, this prove that the Ni atom dissolves in the iron lattice entirely.This indicates the formation of a solid solution of Fe (Ni). For Fe-Cu-Ni powder mixture characteristics. We are seeing that the copper peaks have completely disappeared, as well as the nickel peaks, and the emergence of three Fe (Ni, Cu) peaks, indicating Ni and Cu atomic penetration into the substitution sites of the Fe lattice and the formation of Fe (Ni, Cu) solid solution [103].

3.2.2. The evolution of the lattice parameter:

The lattice parameters of the obtained phases were calculated for most intense plane (hkl) (110) according to the equation below [104]:

$$\frac{1}{d^2} = \frac{h^2+k^2+l^2}{a^2} \qquad (3.1)$$

Where:

d_{hkl}:is interreticular distance

a:is the lattice parameters

(h, k, l):are Miller indices

The figure 3.3 displays the change in lattice parameters as the Cu/Ni ratio changes. It demonstrates that the value of the lattice parameters goes through five variations. As can be seen, the variation is constant for $Fe_{70}Cu_{30}$ and $Fe_{70}Cu_{20}Ni_{10}$ with a= 2.8664 Å, reaches its maximum value for $Fe_{70}Cu_{15}Ni_{15}$ with lattice parameter≈ 2.8671 Å, then decreases to its starting point which is 2.8664 Å at $Fe_{70}Cu_{10}Ni_{20}$, then continues decreases until it reaches the minimum value for $Fe_{70}Ni_{30}$with 2.8638 Å . The increase in the lattice parameter is caused by alloy disordering. Furthermore, the increment in lattice parameter might relate to the accumulation of lattice imperfections in the process of continuous fracture and re-welding of the powder [105]. The decrement in lattice parameter was due to triple defect disorder and the comparatively smaller atomic diameter of Ni and Fe (0.124nm and 0.126nm respectively) than that of Cu (0.225nm).

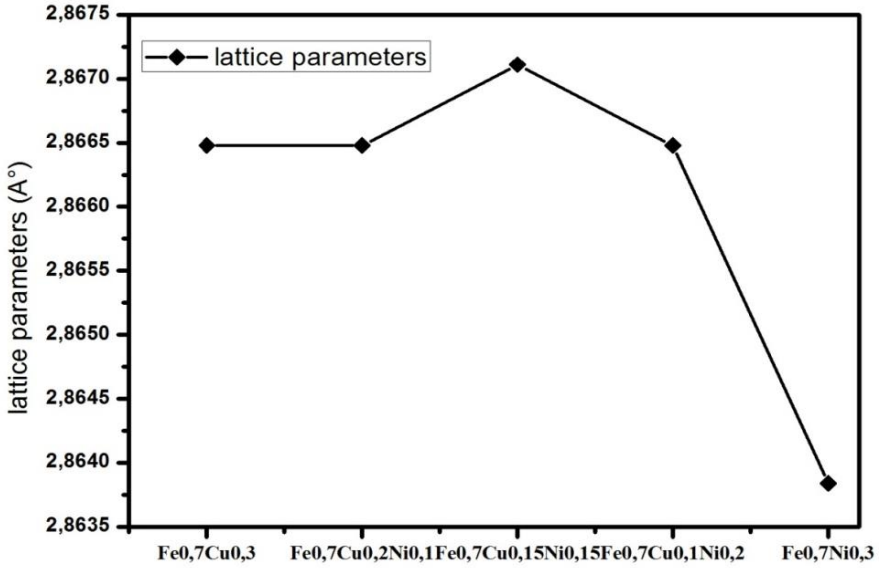

Figure 3.3.Lattice parameter change for different Cu/Ni ratio.

3.2.3. Lattice strain and crystallite size evolution:

Among mechanical alloying powder parameters, the crystallite size (D) and lattice strain (ε) are important parameters in structural characterisation. Both of them can be obtained using X-ray diffraction diffractometer.

The variation in crystallite size of the powder alloy was estimated using the Debye-Scherrer equation by broadening XRD peaks [106]:

$$\boldsymbol{D = \frac{k\lambda}{\beta \cos\theta}} \qquad (3.2)$$

Where:

β: is the full width at half maximum (FWHM) of the diffraction peak.

k: is a dimensionless shape factor.
λ: is the X-ray wavelength.
θ: the Bragg angle.

The lattice strain (ε) is calculated using the equation bellow [106]:

$$\boldsymbol{\varepsilon = \frac{\beta_S}{4\,tan\theta}} \qquad (3.3)$$

Where:

β_S: is the Full width at half maximum

Figure 3.4 shows the evolution of the crystallite size and lattice strain as the Cu/ Ni ratio changes. It was observed that a decrease in crystallite size was found to be accompanied by the increase in the lattice strain.

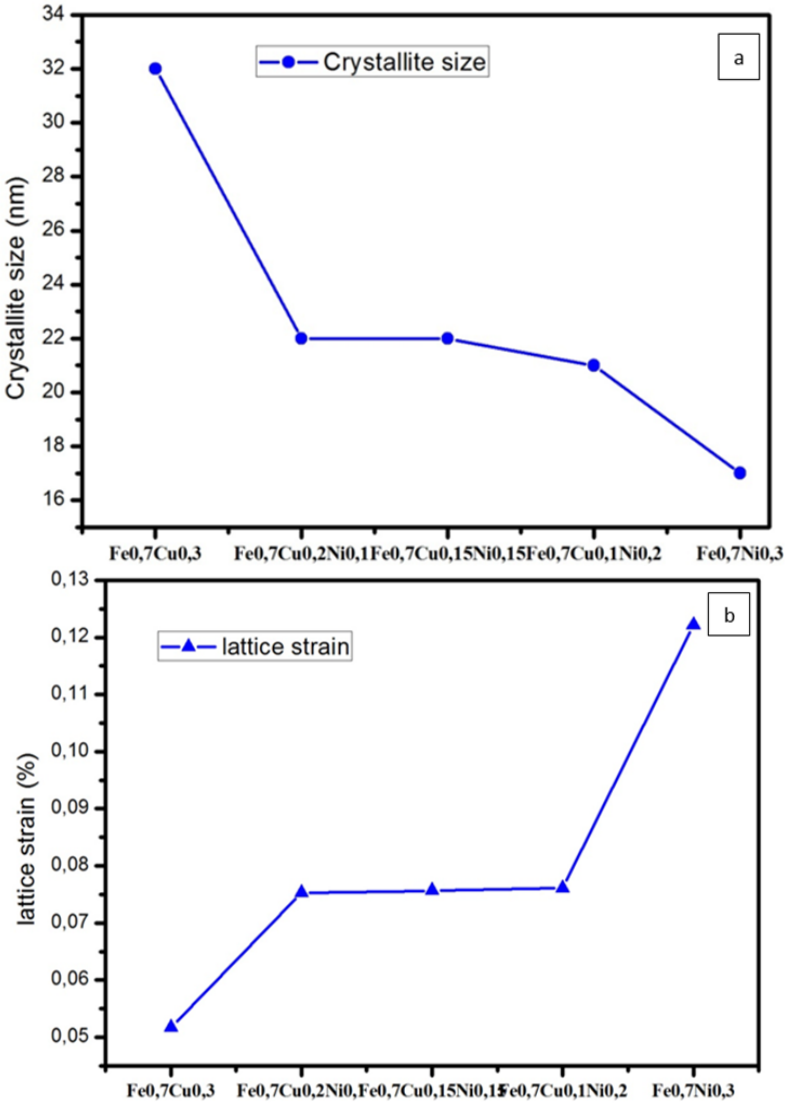

Figure 3.4.Evolution of (a) crystallite size and (b) lattice strain

Figure 3.4 (a) depicts the evolution of crystallite size D (nm) as the Cu/Ni ratio changes. It is remarkable that crystallite size decreases as a function of the Ni content increment, as Hamzaoui et al. showed in [107].

Figure 3.4 (b) shows the evolution of the lattice stain with a different Cu/ Ni ratio. The lattice strain is lowest in the FeCu powder alloy, then increases and stabilises at 0.075 % in Fe Cu Ni powder alloys. Then increase once more until it reaches the maximum value for Fe Ni alloy.

The decrement of crystallite size D and the increment of lattice strain ε was due to the fact that, during the MA, the powder particles are subjected to serve mechanical deformation and are cold welded and fractured, resulting in the refinement of crystallite size as well as an increase in the lattice strain [102].

3.3. Morphology of Fe-Cu-Ni powder alloy:

3.3.1. SEM image:

Figure 3.5 shows a SEM micrograph of the powder from all samples. The difference in the morphology and size of the powders after 10 hours of milling is obvious.

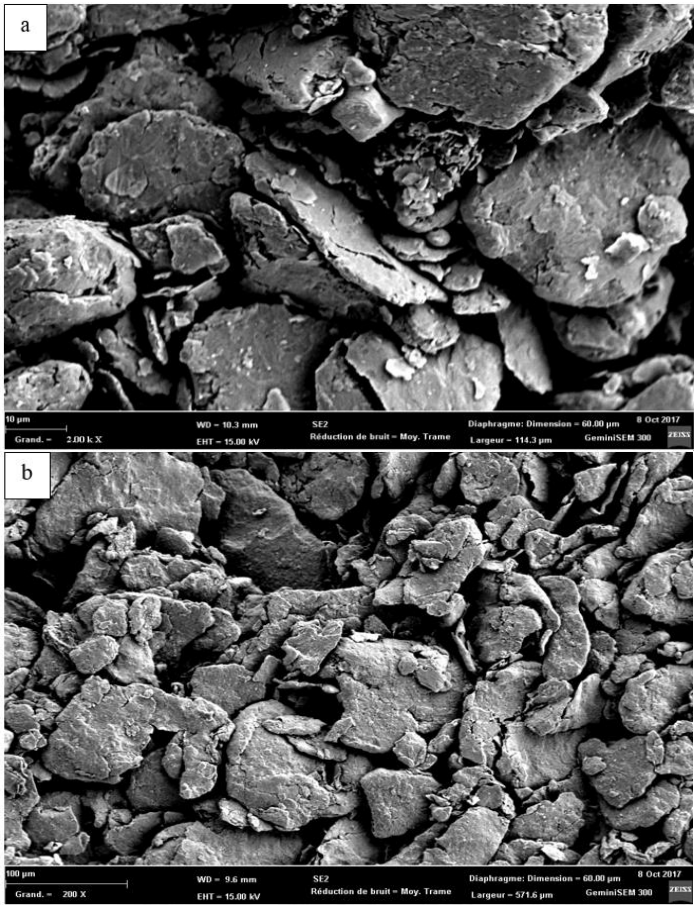

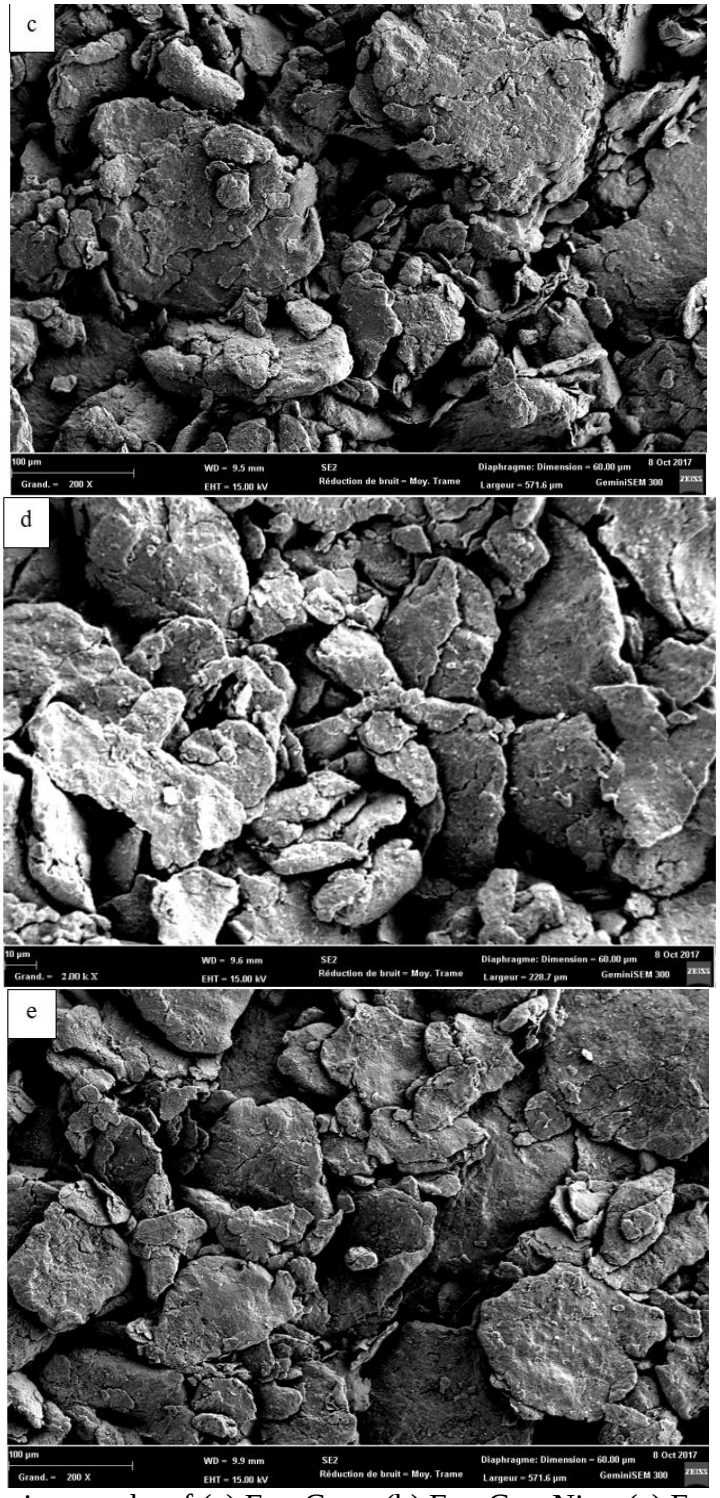

Figure 3.5.SEM micrographs of (a) $Fe_{0.7}Cu_{0.3}$, (b) $Fe_{0.7}Cu_{0.2}Ni_{0.1}$, (c) $Fe_{0.7}Cu_{0.15}Ni_{0.15}$, (d) $Fe_{0.7}Cu_{0.1}Ni_{0.2}$, (e) $Fe_{0.7}Ni_{0.3}$

As can be seen, the powder particles appear flattened and odd in shape, with a plate or lamellar like structure, and are evenly distributed because of the mechanical alloying. The flat shape of the powder particles could be attributed to the strong plastic deformation that occurs at the start of the milling process [108]. In addition, agglomerated particles were observed,

which could be attributed to the welding of small particles on the surface of bigger ones during MA [108].

3.3.2. EDS analysis:

The EDS analysis was used to estimate the concentration of each element that formedforme the powder mixture. EDS analysis of FeCuNi powder alloy as a function of Cu/Ni ratio (figure 3.6.). The results of the EDS spectral quantification show the presence of all the elements that constitute the initial mixture, as well as the absence of all impurities, indicating that the mixture is not contaminated from the atmosphere or milling tools.

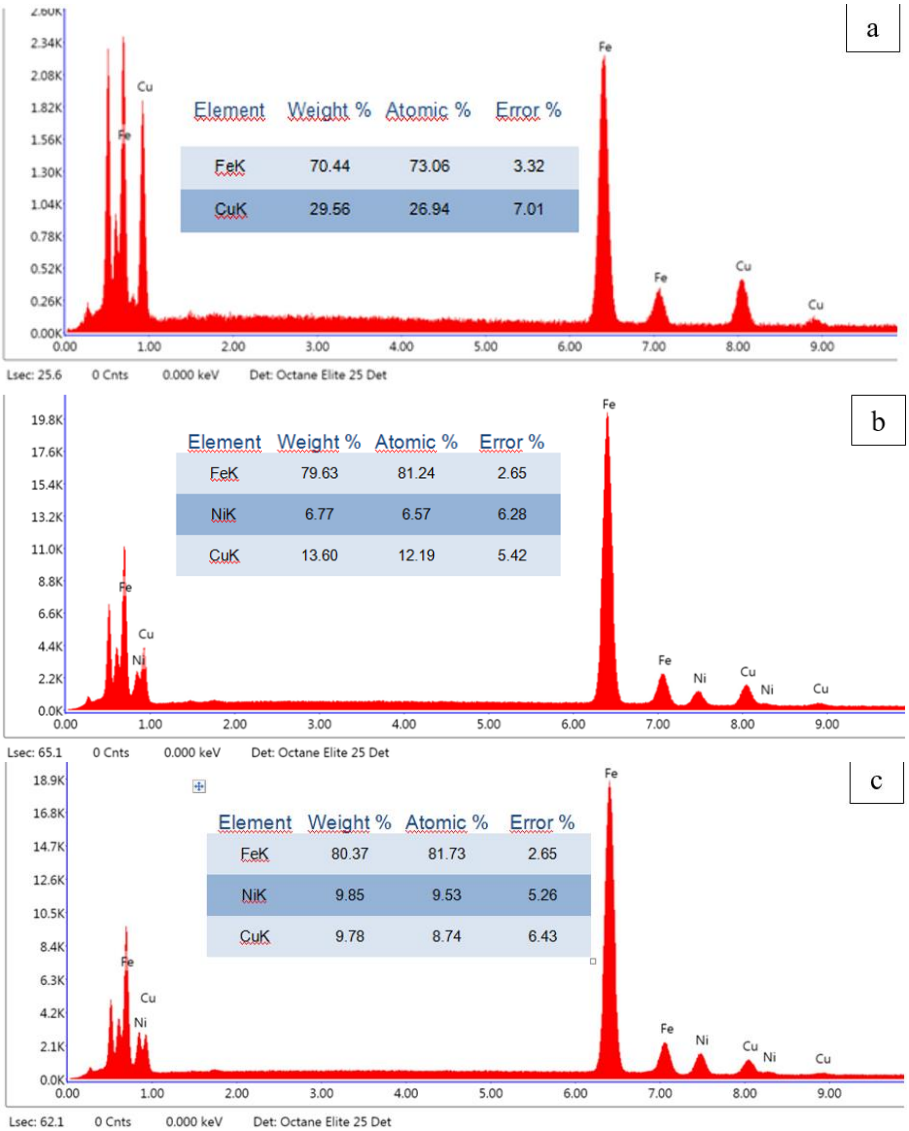

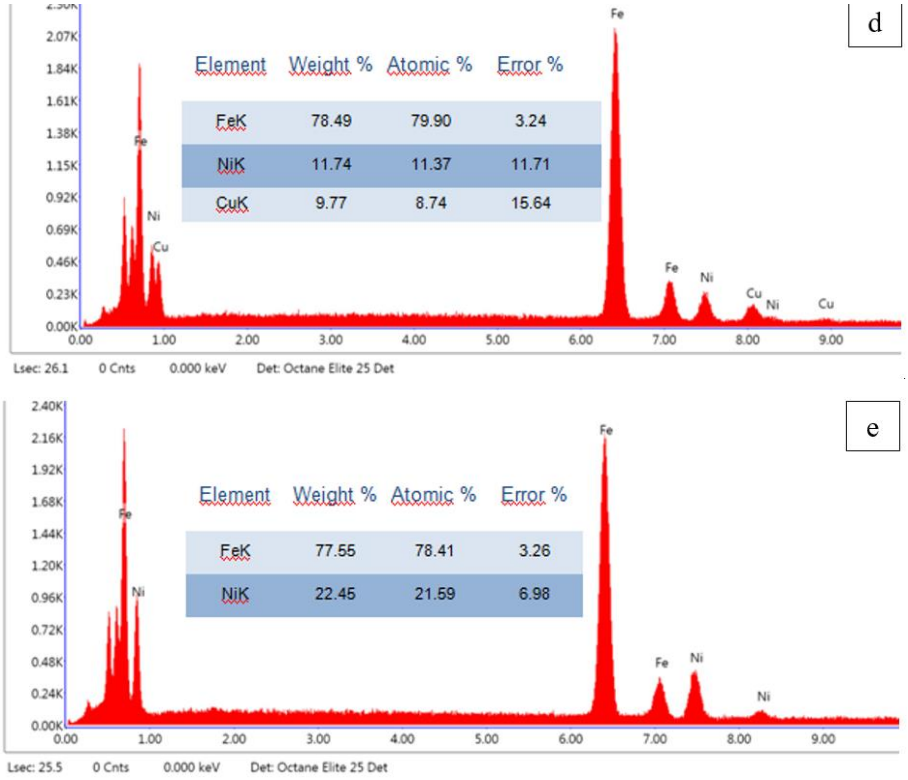

Figure 3.6.Energy dispersive X-ray analysis (EDX) spectrum (a) $Fe_{0.7}Cu_{0.3}$, (b) $Fe_{0.7}Cu_{0.2}Ni_{0.1}$, (c) $Fe_{0.7}Cu_{0.15}Ni_{0.15}$, (d) $Fe_{0.7}Cu_{0.1}Ni_{0.2}$, (e) $Fe_{0.7}Ni_{0.3}$

3.3.3. EDS mapping:

The mechanically alloyed powders were subjected to elemental mapping using EDS. Figure 3.7 depicts a mapping of $Fe_{70}Cu_{30-x}Ni_x$ (x=0, 10, 15, 20, 30) distribution, indicating that the elemental distribution of powder particles is closely correlated and homogenous. As a result, it was estimated that a solid solution had been formed for Fe (Cu), and Fe (Ni, Cu) and Fe (Ni) [109].

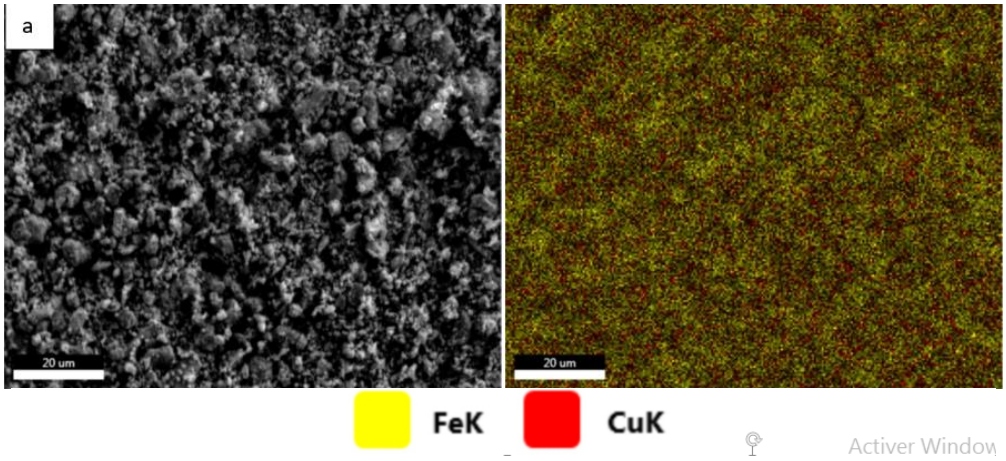

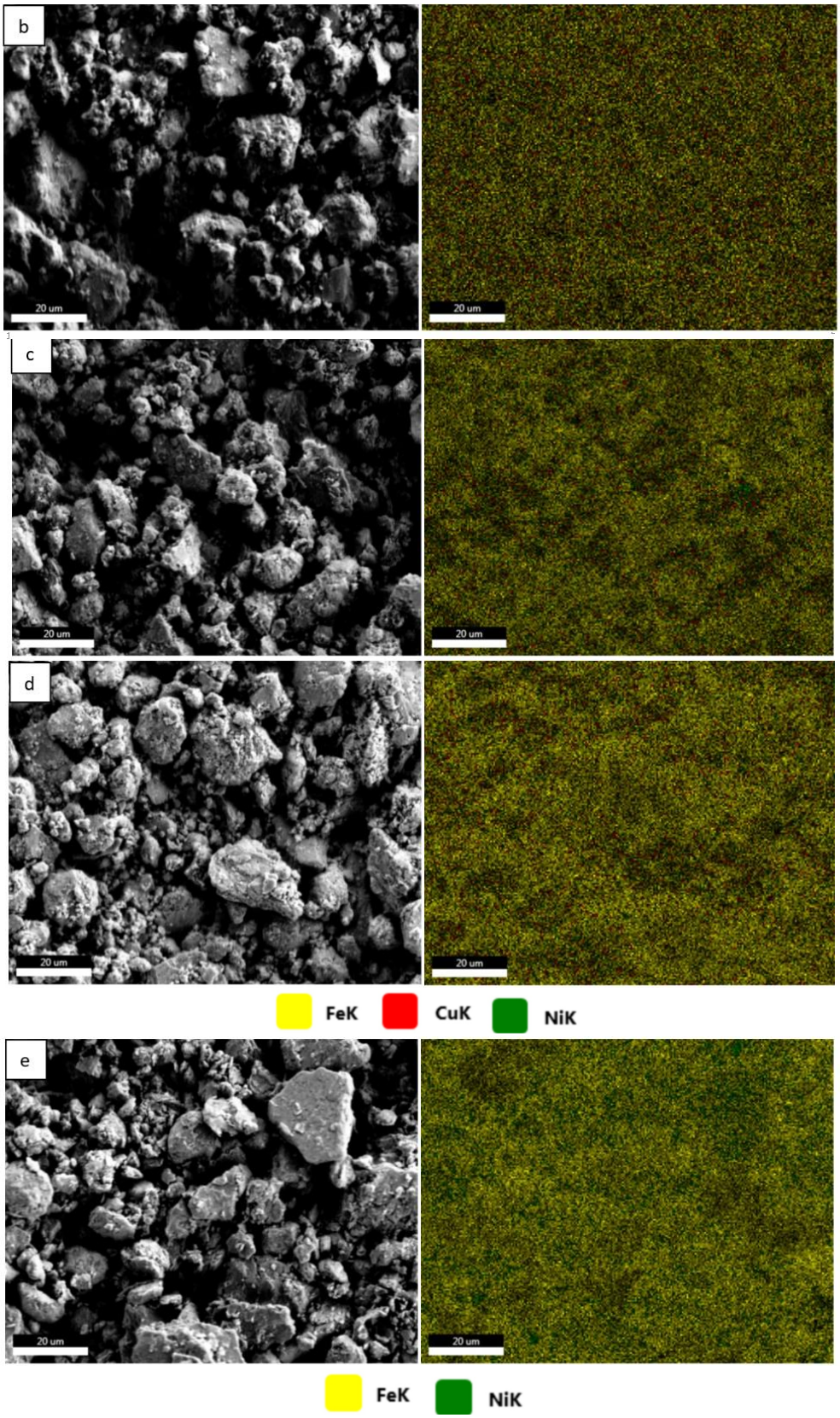

Figure 3.7.EDS mapping of (a) $Fe_{0.7}Cu_{0.3}$, (b) $Fe_{0.7}Cu_{0.2}Ni_{0.1}$, (c) $Fe_{0.7}Cu_{0.15}Ni_{0.15}$, (d) $Fe_{0.7}Cu_{0.1}Ni_{2}$, (e) $Fe_{0.7}Ni_{0.3}$ milled for 10h

3.4. Magnetic characterisation:

The magnetic properties of Fe-Cu-Ni ternary alloys, such as saturation magnetization (Ms), coercivity (Hc), and remanent magnetization (Mr), were investigated using VSM at room temperature under -20 kOe < Hc< 20 kOe conditions. Figure 3.8 shows the magnetic hysteresis loop (magnetization vs. applied field) of Fe Cu Ni alloy with a varying Cu/Ni concentration, obtained at room temperature. The hysteresis loop displays the characteristics of soft magnetic materials, which are high: saturation magnetic flux density, high permeability, low coercivity, and low remanence, all desirable properties in soft magnetic applications [110,111].From figure 3.8, we have deduced the values of the saturation magnetization (Ms), the coercive field (Hc), and the remanence (Mr) that corresponds to the different Cu/Ni concentrations.

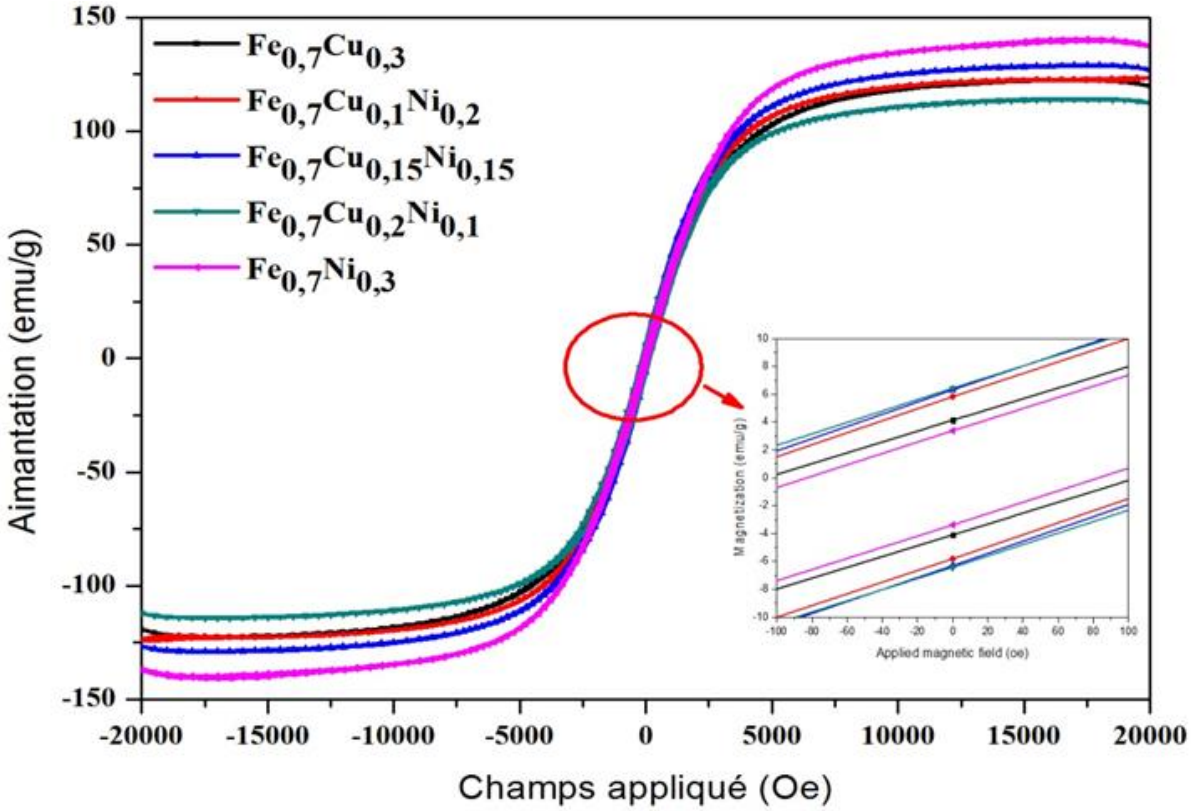

Figure 3.8.Hysteresis loop of Fe-Cu-Ni powders mixture milled for 10 h.

The evolution of Ms of $Fe_{70}Cu_{30-x}Ni_x$ after 10 hours of milling is depicted in figure 3.9. Due to the high magnetic properties of Ni compared to Cu, Ms reaches its maximum value of 140 (emu/g) for the Fe Ni due to the strong influence of chemical composition on saturation magnetization [112]. Meanwhile, we noted a slight decrease in M_s for FeCu. Concerning theFeCuNi nanostructured alloy, Msreaches a maximum value of 15% of Cu then decreases, suggesting a change in magnetic ordering, which can be attributed to the diamagnetic nature

of Cu in the structure. Furthermore, the increase in magnetization is correlated to the increase in lattice strain and the introduction of deferent default during mechanical milling.

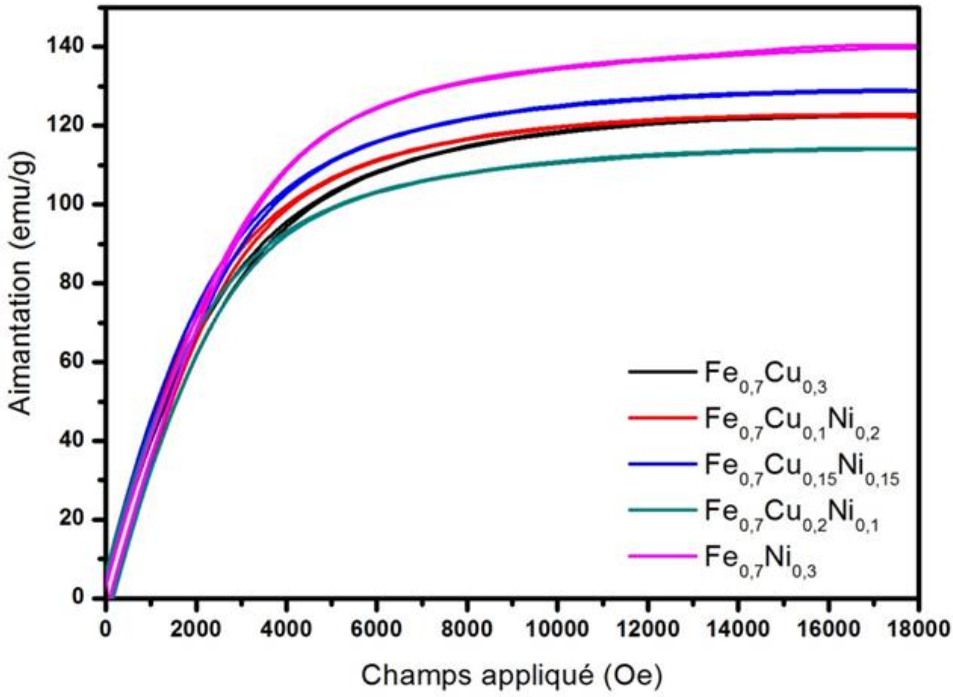

Figure 3.9.Evolution of Ms of FeCuNi at 10 h of milling

Figure 3.10 depicts the evolution of the coercive field Hc for $Fe_{70}Cu_{30-x}Ni_x$ milled for 10 h.

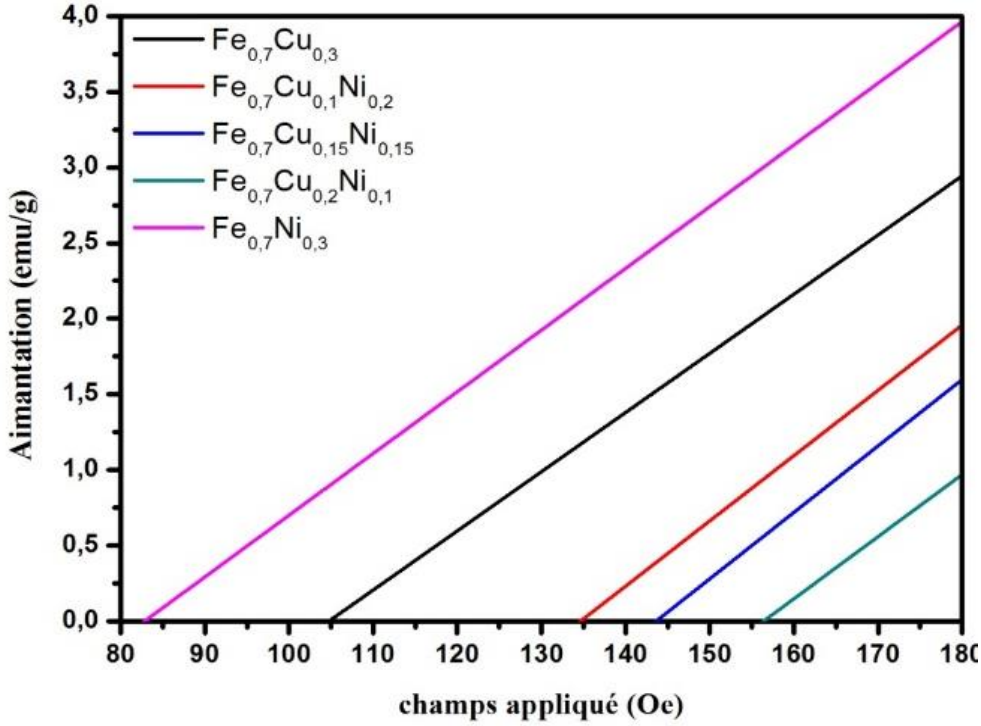

Figure 3.10.Evolution of Hc of Fe-Cu-Ni at 10 h of milling

The increment in coercivity can be explained by the introduction of different types of defects, the increase in internal strain, and the insertion of copper atoms into theFeNi lattice due to the severe plastic deformation caused by the mechanical milling, which serve as pinning sites for the magnetic domain wall movement. Furthermore, the crystal anisotropy, shape anisotropy and magneto-static interactions and magneto-crystalline anisotropy play a vital role that stimulates the magnetic properties [113].

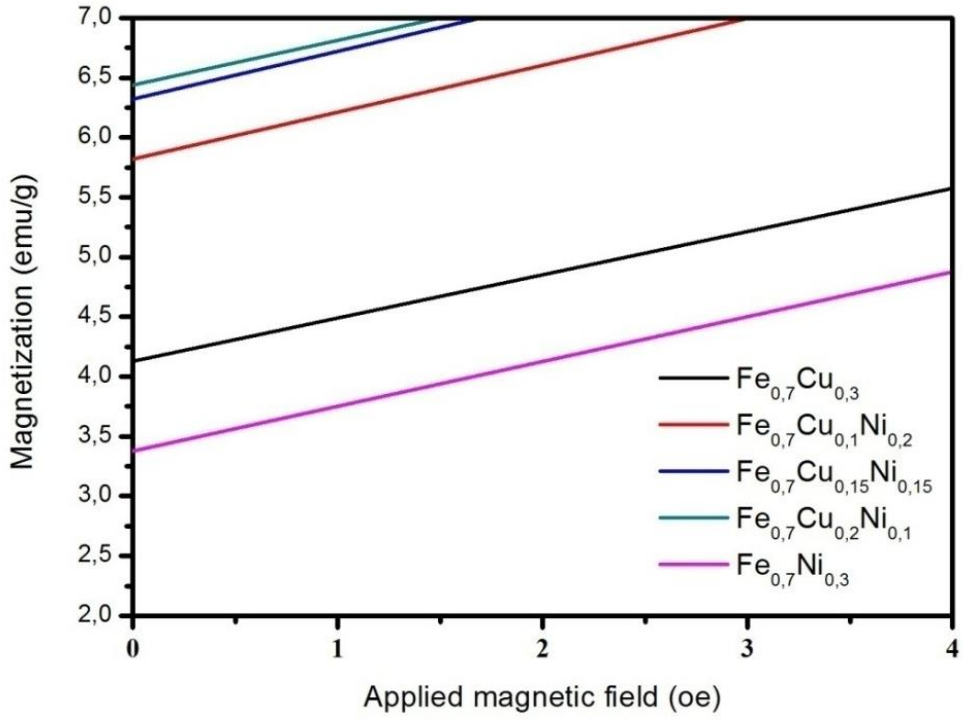

Figure 3.11.Evolution of Mr of FeCuNi at 10 h of milling

The evolution of the remanent magnetisation of the $Fe_{70}Cu_{30-x}Ni_x$ alloy milled for 10h is shown in figure 3.11. We remark that the remanent magnetisation of FeCu nanostructured alloy is greater than that of FeNi nanostructured alloy, as well as the addition of Cu with FeNi, will increase the remanent magnetization and also it increases with the increase in Cu concentration. The remanent magnetisation increased as a function of increasing Cu concentration in the $Fe_{70}Ni_{30-x}Ni_x$ nanostructured alloy. Copper, which is diamagnetic, with an atomic radius greater than Fe and Ni, suppresses the alignment of the magnetic moments of Fe and Ni.

CONCLUSION

Mechanical alloying is an interesting elaboration technique compared to other traditional procedures due to its low cost and speeds of execution. It is a high-energy milling method for obtaining alloyed powders via solid-state processes. It consists mostly of repeated collisions that cause fractures and cold welding of powder particles trapped between milling balls. The Fe-Ni-Cu nanostructured powders were successfully elaborated by the PM400 planetary mill.

The milling of the powders revealed the stages of the mechanism of formation of the different phases of the alloy. Firstly, in the Fe-Cu alloy, we notice that the copper is gradually being introduced into the structure of the iron. As for the Fe-Ni alloy, the nickel dissolves in the iron lattice entirely, which indicates the formation ofsolid solution Fe (Ni).

The XRD spectra showed that the Fe (CuNi) solid solution is formed after 10h of milling. The crystallite size decreases and lattice strain increases as a function of the increment of the Ni content until it reaches the values of 17nm and 0.12%, respectively. In parallel to this, thelattice parameter increases until it reaches its maximum value for $Fe_{70}Cu_{15}Ni_{15}$ with a lattice parameter$\approx$ 2.8671 Å.

The study of the morphology of the powder allowed us to observe the change in the shape and size of the particles after milling; it has been noticed through EDS that the structure is homogenized, which means that the alloy has probably been formed.

The VSM characterisation allowed us to determine the magnetic properties. These properties provide information on the structural state of the samples and are confirmed by classical methods (SEM and XRD). In addition, the analysis of Hc, Mr and Ms obtained from the hysteresis cycles gave us information on the magnetic aspect of the structures obtained after milling. We have noticed that Ms reaches its maximum value of 140 (emu/g) because of the influence of the chemical composition on saturation magnetisation. This increase in Ms could be attributed to the formation of a solid solution.

The increase in coercsivity is due to the reduction of the grain size and the introduction of different types of defects.

In perspective, we hope to develop the mechanical alloying of the Fe-Ni-Cu system by varying the milling time and conditions (the speed, the ball/powder mass ratio, the alloy composition) and to deepen the study concerning the stress aspect of the structures formation.

We also hope to use these milled powder mixtures as coatings on steel substrates and to study their different properties.

List of symbols and abbreviations	
STM	**Scanning Tunnelling microscope.**
0-D	**Zero Dimension.**
1-D	**One Dimension.**
2-D	**Two Dimension.**
3-D	**Three Dimension.**
CNTs	**Carbon Nanotubes.**
CNFs	**Carbon Nanofibers.**
Nm	**Nanometre.**
MRI	**Magnetic Resonance Imaging.**
SPIO	**Super Paramagnetic Iron Oxide.**
CVD	**Chemical Vapour Deposition.**
PVD	**Physical Vapour Deposition.**
MA	**Mechanical Alloying.**
ODS	**Oxide Dispersion-Strengthened alloys.**
INCO	**International Nickel Company.**
PCA	**Processing Control Agent.**
HVOF	**High-Velocity Oxy-Fuel flame.**
TBCs	**Thermal Barrier Coatings.**
SOFC	**Solid Oxide Fuel Cells.**
THE	**High-Temperature Electrolyser.**
CGDS	**Cold Gas Dynamic Spraying.**
D.C	**Direct Current.**
APS	**Atmospheric Plasma Spraying.**
VPS	**Vacuum Plasma Spraying.**
R.F	**Radio Frequency**
SEM	**Scanning Electron Microscope.**
EDS/EDS	**X-ray Energy Dispersive Spectroscopy.**
TEM	**Transmission Electron Microscope.**
ETD	**Everhart-Thornley Detector.**
BSE	**Backscattered Electron.**
SE	**Secondary Electron.**
PTS	**Position-Tagged Spectrometry.**

List of symbols and abbreviations	
XRD	**X-Ray Diffraction.**
AFM	**Atomic Force Microscope.**
VSM	**Vibrating Samples Magnetometer.**
M	**Magnetizing force.**
B	**Magnetic flux density.**
C	**Material Constant.**
T	**Temperature.**
T_C	**Curie Temperature.**
B	**Full Width Of Half Maximum (FWHM).**
K	**Dimensionless shape factor.**
θ	**Bragg angle.**
λ	**X-ray wavelength.**
E	**Lattice strain.**
D	**Crystallite size.**
M_s	**Saturation Magnetization.**
H_C	**Coercivity.**
M_r	**Remanent Magnetization.**
Fe	**Iron**
Cu	**Copper**
Ni	**Nickel**

REFERENCES

[1] Nasirpouri, N. “Electrodeposition of nanostructured materials”, Springer Series in Surface Sciences, 2017 vol 62, pp. 1-42.

[2] J. A. Scher, J. M. Elward, A. Chakraborty,“A. Shape matters: effect of 1D, 2D, and 3D isovolumetric quantum confinement in semiconductor nanoparticles”, The Journal of Physical Chemistry C, 2016, pp.1.

[3]Cherie R. Kagan, Christopher B. Murray,“Charge transport in strongly coupled quantum dot solids”, journal Nature Nanotechnology, 2015, pp. 1.

[4] El-Eskandarany M, Aoki K, Suzuki K, “Solid State Amorphizing Reaction of $Al_{30}Ta_{70}$ alloy powders by the rod milling technique”, Journal of the Japan Society of Powder and Powder Metallurgy, 1991vol38(1), pp.62-95.

[5] Sherif El-Eskandarany M,“Mechanical solid state mixing for synthesizing of SiCp/Al nanocomposites”, Journal of Alloys Compounds,1998vol 279 (2),pp. 263-271.

[6] M. SherifEl-Eskandarany, F. Itoh, K. Aoki, K. Suzuki, “Preparation of Al_xTa_{1-x} amorphous alloy powder by mechanical alloying”, journal of Non-Cryst. Solids, 1990 vol 117-118, pp. 32-729.

[7] Coraline Crozet. “Equilibres de phases et microstructures d’alliages Cu-Fe-Ni riches en Fe ”. Autre. Université de Grenoble, 2011, pp. 3.

[8] N. Castin, L. Malerba, G. Bonny, M.I. Pascuet, M. Hou, “Modelling radiation-induced phase changes in binary FeCu and ternary FeCuNi alloys using an artificial intelligence-based atomistic kinetic Monte Carlo approach”, Nuclear Instruments and Methods in Physics Research B, 2009vol267 (18), pp. 1-7.

[9]Ke Liu, Li-Juan Hu, Qiao-Feng Zhang, Yao-Ping Xie, Chao Gao, Hai-Ying Dong, Wan-YiLiang, “EffectofNi and vacancyconcentration on initialformationofCuprecipitate in Fe–Cu–Ni ternaryalloys by moleculardynamics simulation” , ChinrsePhysics B, 2017vol 26 (8), pp. 1-7.

[10] A.T. Al-Motasem, M. Posselt, F. Bergner, “Nanoclusters in bcc-Fe containing vacancies, copper and nickel: structure and energetics”, Journal of Nuclear Materials, 2011, pp. 215-222.

[11] Kent JA. “Handbook of Industrial Chemistry and Biotechnology”, SpringerScience+Business, 2012 Vol. 1, pp. 265.

[12]D Brabazon, “Nanostructured Materials”, Elsevier, 2016, pp.1.

[13] European Commission. “Nanosciences and Nanotechnologies: An action plan for Europe”, 2005–2009. Office for Official Publications of the European Communities, 2009; 2005.

[14] The Project on Emerging Nanotechnologies. 2014. Consumer products inventory. Available at http://www.nanotechproject.org/cpi/. Accessed 2015 Oct 14.

[15] Dieter Vollath, “Nanomaterials: An Introduction to Synthesis, Properties and Applications”, 2013, pp. 1.

[16]Louis Laurent, Jacques Villain, “Nanoscience and nanotechnologies: hopes and concerns”, 2011 Volume 12, pp. 601-702.

[17] Pautrat, J.-L. “Nanosciences: Evolution or revolution? ”, Comptes Rendus Physique, 2011 vol 12(7), pp. 605–613.

[18]Calugaru, V., Magné, N., Hérault, J., Bonvalot, S., Le Tourneau, C., &Thariat, J, “Nanoparticules et radiothérapie. Bulletin Du Cancer”, 2015 vol102(1), pp. 83–91.

[19] Saini S, Stark D. D, Hahn P. F, Wittenberg J, Brady T. J, Ferrucci JT,“Ferrite particles: a superparamagnetic MR contrast agent for the reticuloendothelial system”. Radiology, 1987.

[20] Kim M. J, Kim J. H, Chung J. J, Park M. S, Lim J. S, Oh Y. T,“Focal hepatic lesions: detection and characterization with combination gadolinium- and superparamagnetic iron oxide-enhanced MR imaging”, Radiology, 2003.

[21] Nanomatériaux : Une revue des définitions, des applications et des effets sur la santé. Comment implémenterundéveloppementsûr.

[22] Zhong W. H, “Nanoscience and Nanomaterials: Synthesis, Manufacturing and Industry Impacts”. DEStech Publications, 2012.

[23] RATNA TANTRA, “Nanomaterial characterization introduction”, 2016, pp. 25.

[24] Tien D, Liao C. Y, Huang J. C, Tseng K. H, Lung J. K, Tsung T. T, Kao W. S, Tsai T. H, Cheng T. W, Yu B.S, “Novel technique for preparing a nano-silver water suspension by the arc-discharge method”, Mater Sci 2008, pp.750-756.

[25] Gogotsi Y, “Nanomaterials Handbook”, Taylor & Francis, 2006.

[26]Bourdon J, “Growth and Properties of Metal Clusters. Applications to Catalysis and the Photographic Process”, Elsevier, 1980,pp. xviii-549.

[27]Lackner M, “Combustion Synthesis: Novel Routes to Novel Materials”, Bentham Science Publishers, 2010.

[28]Cao G, “Nanostructures and Nanomaterials Synthesis, Properties and Applications”, World Scientific, 2004, pp. 184-189.

[29]TripathiN, Mishra P, Joshi B, Islam SS, “Precise control over physical characteristics of carbon nanotubes by differential variation of Argon flow rate during chemical vapor deposition processing: A systematic study on growth kinetics”, Mater SciSemicond Process 2015, pp. 207-215.

[30] Turkevich J, Stevenson PC, Hillier J, “A study of the nucleation and growth processes in the synthesis of colloidal gold”, Discuss Faraday Soc, 1951 vol11(0), pp. 55-75.

[31]Rao C. N. R, Thomas P. J, Kulkarni G. U, “Nanocrystals: Synthesis, Properties and Applications”, Springer, 2007 Vol. 95, pp. 25-68.

[32]Kumar C, “Mixed Metal Nanomaterials(Nanomaterials for the Life Sciences)”, Wiley-VCH, 2009, pp. 281.

[33]Robert Corriu, Nguyen TrongAnh,“Molecular Chemistry of Sol–gel Derived Nanomaterials”, Wiley, 2009, pp.38-41.

[34]Lisa Klein, Mario Aparicio, Andrei Jitianu,“Handbook of sol–gel science and technology: Processing, Characterization and Applications, vol.1, 1: Sol–gel processing,”Kluwer Academic,2004, pp.3-5.

[35]Li Yimin, Somorjai, Gabor A,“Nanoscale advances in catalysis and energy applications”. Nano Letters,2010 vol 10 (7), pp.2289-2295.

[36]Lu K, “Nanoparticulate Materials: Synthesis, Characterization, and Processing”. John Wiley & Sons, 2012.

[37]Hartanto A. B, Ning X, Nakata Y, Okada T, “Growth mechanism of ZnOnanorods from nanoparticles formed in a laser ablation plume”, Applied Physics A: Materials Science and Processing, 2004 vol 2 (78), pp. 299-301.

[38]Takeshi Tsuji, D. H Thang, Yuuki Okazaki, Masataka Nakanishi, YasuyukiTsuboi, Masaharu Tsuji, “Preparation of silver nanoparticles by laser ablation in polyvinylpyrrolidone solutions”, Applied Surface Science, 2008 vol 254(16), pp. 5224-5230.

[39]Benjamin J. S, “Mechanical Alloying”,Journal Scientific American, 1976, pp. 40-49.

[40]El-Eskandarany M. S, Aoki K, Suzuki K, “Rod milling for Solid-state formation of $Al_{30}Ta_{70}$ amorphous alloy powder”,Journal of Less Common Metals, 1990 Vol 167 (1), pp. 113-118.

[41] P.S. Gilman, J.S. Benjamin, “Mechanical Alloying”, Annual Reviews Mater Sci,1983 Vo1.13. pp. 279.

[42] J.S. Benjamin, “Novel Powder Processing Adv. In Powder Metall”, Publ. Metal Powder Inductries, 1992 Vol. 7, pp. 155.

[43] Benjamin J.S, “Mechanical Alloying- a perspective”, Metal Powder Rep 1990, vol45:122-7.

[44] Benjamin J. S, “Dispersion strengthened superalloys by mechanical alloying”, Metallurgical Transactions, 1970, pp. 2943-2951.

[45] Koch C. C, Cavin O. B, McKamey C. G, Scarbourgh, J. O, “Preparation of amorphous $Ni_{60}Nb_{40}$ by mechanical alloying”, Appl. Phys. Lett, 1983.

[46]White, R. L, “The Use of Mechanical Alloying in the Manufacture of Multifilamentary Superconductor Wire”, Ph.D. Thesis, Stanford University 1979.

[47] H. Kimura, M. Kimura, T. Ban, “Proceeding of the 2nd International Conference on Rapidly Solidified Materials”, ASM International, M 1988, pp. 172.

[48] W.E. Kuhn, “In: Modern Developments in Powder Metallurgy”, MPIF, Princeton, N.J. 1980vol12, pp.195.

[49] A.N. Patel, W.E. Kuhn, “In: Modern Development in Powder Metallurgy”, MPIF, Princeton, N.J. 1980 vol13, pp.2750.

[50] G.B. Schaffer, P.G. McCormick,“Ananocrystalline mixture of intermetallic compounds by mechanical alloying”, Metall. Trans. Forum. A23 1992.

[51] C. Suryanarayana, “Mechanical alloying and milling Progress in Materials Science”,2001vol 46, pp. 1-184.

[52] C. Suryanarayana, “Mechanical Alloying and Milling”, (2004), pp. 39.

[53]M. Sherif El-Eskandarany, “Mechanical Alloying For Fabrication Of Advanced Engineering Materials”, Noyes Publications, 2001, pp. 8.

[54] K. Murakami, K. Mino, H. Harada, H. K. D. H. Bhadeshia, “Nonuniformn recrystallization in a mechanically alloyed Nickel-Base superalloy”, MetallurgicalTransactions, (1993)vol 24A, pp. 1049.

[55] W. Sha, H.K.D.H. Bhadeshia, Metallurgical and Material Transactions, (1994)vol 25A, pp. 705.

[56] Davis R.M, Koch C.C, “Mechanical alloying of brittle components: silicon and germanium”,ScriptaMetall, 1987 vol 21, pp. 10.

[57] Lee P. Y, Koch C. C, “Formation of amorphous Ni-Zr alloys by mechanical alloying of mixtures of the intermetallic compounds $Ni_{11}Zr_9$ and $NiZr_2$”, Applied Physics Letters, 1987 vol 50 (2), pp. 1578-80.

[58] White R. L, “the Use of Mechanical Alloying in the Manufacture ofMultifilamentary Superconductor Wire”, Ph.D. Thesis, Stanford University 1979.

[59] Rainer Birringer, H. Gleiter, H-P. Klein, P. Marquardt, “Nanocrystalline materials an approach to a novel solid structure with gas-like disorder”, Physics Letters A, 1984 Vol 102 (8), pp. 365-369.

[60] Kenji Amiya, Nobuyuki Nishiyama, A Inoue, T Masumoto, “Mechanical strength and thermal stability of Ti-based amorphous alloys with large glass-forming ability”,Materials Science and Engineering A, 1994 vol 179, pp. 57.

[61] Z. G. Li, David J. Smith, “observations of nanocrystals in thin TbFeCo films”, Applied Physics Letters, 1989 vol 55 (9), pp. 919.

[62] B.H. Kear, P.R. Strutt, “Chemical processing and applications for nanostructured materials”, Nanostructured materials, 1995vol 6, pp. 227.

[63] H. Gleiter, “Nanostructured materials: state of the art and prespective”, Nanostructured materials, 1995 vol 6, pp. 3-14.

[64] C.C. Koch,“The synthesis and structure of nanocrystalline materials produced by mechanical attrition: A review”, Nanostructure Materials, 1993vol 2 (2), pp. 109.

[65] C.C. Koch, “Synthesis of nanostructured materials by mechanical milling: problems and apportunities”,Nanostructured Materials, 1997 vol 9, pp. 13.

[66] Xuan Li, ZeanTianb, QuanXie, Kejun Dong, “The topologically close-packed $Fe_{70}Cu_{15}Ni_{15}$ nanoparticles- A simulation study”, Vacuum 193, 2021.

[67] Jingjing Li, Zean Tian, QuanXie, ShixianXiong, “Component effect on microstructure of rapidly cooled FeCuNi alloys”, Chemical Physics Letters 753, 2020.

[68] Qiongyu Zhou, Yi Wang and QingdongZhong, “Electrochemical studies on the passivation behavior of Cu-Ni-Fe alloy in borate buffer solution at pH 8.4”, Trans Tech Publications, Switzerland, 2012.

[69] A. Younes, N. Dilmi, M. Khorchef, A. Bouamar, N-E. Bacha, M. Zergoug, “Structural and magnetic properties of FeCuNi nanostructured produces by mechanical alloyin”, 2018.

[70] Coraline Crozet, “Equilibres de phases et microstructures d’alliages Cu-Fe-Ni riches en Fe”, thèse de Doctorat, Grenoble, 2006.

[71] S. Cazottes, A. Fnidiki,M. Coisson, D. Lemarchand, F. Danoix, “Correlation between microstructure at fine scale and magnetic properties of magnetoresistive $Cu_{80}Fe_{10}Ni_{10}$ ribbons: Modeling of magnetization”, Journal of Magnetism and Magnetic Materials, Volume 333, May 2013, Pages 22-29.

[72] C. Zhang, M. Enomoto, “Study of the influence of alloying elements on Cu precipitation in steel by non-classical nucleation theory”,ActaMaterialia, 2006 vol 54, pp. 4183-4191.

[73] Y.P. Xie, S.J. Zhao, “The energic and structural properties of BCC NiCu, FeCu alloys: A first-principle study, Computational Materials Science, 2011 vol 50, pp. 2586–2591.

[74] Boutareg Smail, Tounsi Djallel Abdenacer, ”Elaboration et caractéristiques des matériaux nanostructures à base de Fe et Ni”, Université Saad Dahlab Blida 1, 2019.

[75] Coraline Crozet. Equilibres de phases et microstructures d’alliages Cu-Fe-Ni riches en Fe. Autre. Université de Grenoble, 2011.

[76] Milone A. F, Ortalli I, Soardo G. P,“Curie temperature of Ni−Fe alloys in the region (24-35) % Ni from Mössbauer experiments”, Il NuovoCimento D, 1(1),1982, pp. 18–20.

[77] NaoumBoudinar,“ Elaboration et etude structurale et microstructurale des poudres nanostructurées à la base de Fer”, thèse de doctorat UniversitéBadjiMokhtarAnnnaba, 2011.

[78] Joseph I. Goldstein, Dale E. Newbury, Joseph R. Michael, Nicholas W.M. Ritchie, John Henry J. Scott, David C. Joy, “Scanning Electron Microscopy and X-Ray Microanalysis”, Fourth Edition 2018, SpringerScience+Business, pp. 7.

[79] Yang Leng, “Materials Characterization: Introduction to Microscopic and Spectroscopic Methods”, Second Edition 2013, Wiley-VCH Verlag GmbH & Co. KGaA, pp. 127.

[80]Haguenau F, Hawkes P.W, Hutchison J.L, Satiat-Jeunemaitre B, Simon G.T, Williams D.B,“Key events in the history of electron microscopy”,Microsc. Microanal, 2003 (9), pp. 96-138.

[81] A. Bogner, P.H. Jouneau, G. Thollet, D. Basset, C. Gauthier, “A history of scanning electron microscopy developments: Towards ‘‘wet-STEM’’ imaging”, Elsevier,2006, pp. 390.

[82] Anwar Ul-Hamid, “A Beginners’ Guide to Scanning Electron Microscopy”, Springer Nature Switzerland AG, 2018, pp. 4.

[83] Anwar Ul-Hamid, “A Beginners’ Guide to Scanning Electron Microscopy”, Springer Nature Switzerland AG, 2018, pp. 95-96.

[84] Anwar Ul-Hamid, “A Beginners’ Guide to Scanning Electron Microscopy”, Springer Nature Switzerland AG, 2018, pp. 234-236.

[85] Heuser, J,“Whatever happened to the ‘microtrabecular concept’?” Biol Cell, 2003 vol 94, pp. 561-596.

[86] Series Editor: Dr Julian Heath, “Energy Dispersive Spectroscopy”, John Wiley & Sons Ltd, 2015,pp. 6.

[87] A.J.Garratt-Reed, D.C.Bell, “Energy-Dispersive X-Ray Analysis in the Electron Microscope”, BIOS Scientific Publishers Limited, 2003, pp. 3.

[88] Series Editor: Dr Julian Heath,“Energy Dispersive Spectroscopy”, John Wiley & Sons Ltd, 2015, pp. 7-8.

[89] M. AbdMutalib, M.A. Rahman, M.H.D. Othman, A.F. Ismail, J. Jaafar. “Scanning Electron Microscopy (SEM) and Energy-Dispersive X-Ray (EDS) Spectroscopy”, Elsevier,2017, pp. 167-168.

[90] Joseph I. Goldstein, Dale E. Newbury, Joseph R. Michael, Nicholas W.M. Ritchie, John Henry J. Scott, David C. Joy, “Scanning Electron Microscopy and X-ray Microanalysis”, Springer, 2013, pp 295.

[91] Warreen, B. E,“X-ray Diffraction”,Reading, Mass.,Addison-Wesley Pub Co, 1969.

[92] Joel Greenberg,X-Ray Diffraction Imaging Technology and Applications, Taylor & Francis Group, 2019, pp. xix-xx.

[93] Cullity, B. D, “Elements of X-Diffraction”, Prentice Hall: Upper Saddle River, NJ, 3rd Ed 2001.

[94] S. Foner, “Versatile and sensitive vibrating-sample magnetometer”, Review of scientific instrumets, 1959vol 30(7), pp. 548-558.

[95] R. V. Krishnan, A. Banerjee, “Harmonic detection of multipole moments and absolute calibration in a sample, low-cost vibrating sample magnetometer”, Review of Scientific Instruments, 1999 vol 70, pp. 85-91.

[96] S. Kundu and T. K. Nath, “An Automated Home Made Low Cost Vibrating Sample Magnetometer”, Department of Physics and Meteorology, Indian Institute of Technology Kharagpur.

[97] Lopez-Dominguez, V. Quesada, A. Guzmán-Mínguez, J. C. Moreno, L. Lere, M.; Spottorno, J. Giacomone, F. Fernández, J. F. Hernando, A. García, M. A, “A simple vibrating sample magnetometer for macroscopic samples”. Review of Scientific Instruments. 2018.

[98] Burgei Wesley,Pechan Michael J, Jaeger Herbert, “A simple vibrating sample magnetometer for use in a materials physics course”, American Journal of Physics, 2003, pp. 819-828.

[99] O'Handley R.C, “Modern Magnetic Materials: Principles andApplications”, John Wiley &Sons, 1999.

[100] Hong Shi, Minghui Liu, Lin Cong, and Lizhong Wang, “A study on preparation and mechanism of Ni based ternary alloy”, American Scientific Publishers, 2019.

[101] M. Gogebakan, B. Avar, “Quasicrystalline phase formation during heat treatment in mechanically alloyed Al65Cu20Fe15 alloy”, Materials Science-Poland, 2009 vol 27, pp. 920-924.

[102] A. Djekouna,Bouzabata, Otmania, J.M. Greneche, “X-ray diffraction and Mössbauer studies of nanocrystalline Fe–Ni alloys prepared by mechanical alloying”, Catalysis Today 89, 2004, pp. 319–323.

[103] D. Oleszak, P.H. Shingu, “Mechanical alloying of FeAl system”, Materials Science and Engineering: A, 1994 vol 181-182, pp. 1217.

[104] Forouzanmehr N, Karimzadeh F, Enayati M.H, “synthesis and characterization of TiAl/α-AlO_3nanocomposite by mechanical alloying”, J.Alloys Compd., 2009 Vol. 478, pp. 275-259.

[105] JileiXiong,ShunkangPan, LichunCheng, XingLiu, PeihaoLin, “Structure and microwave absorption properties of Pr–Fe–Ni alloys”, Journal of Magnetism and Magnetic Materials384, (2015), pp. 106-112.

[106] C. Suryanarayana, M. Grant Norton, “X-ray Diffraction A Practical Approach, Plenum Press”, New York (1998), pp. 207.

[107] R. Hamzaoui, O. Elkedim, N. Fenineche, E. Gaffet, J. Craven, “Structure and magnetic properties of nanocrystalline mechanically alloyed Fe–10% Ni and Fe–20% Ni”, Materials Science and Engineering: A 360(1-2),2003,pp. 299-305.

[108] M. Slimi, M. Azabou, L. Escoda, J.J. Sunol, M. Khitouni, “Structural and microstructural properties of nanocrystalline Cu-Fe-Ni powders produced by mechanical alloying”,Powder Technology,2014.

[109] Wei Lu, Yewen Xu, Jindan Shi, Song, Xiang Li, “Soft magnetic properties and giant magnetoimpedance effect in thermally annealed amorphous $Co_{68}Fe_4Cr_3Si_{15}B_{10}$”, Jouranl of Alloys and Compounds, 2015 vol 638, pp. 233-238.

[110] G.E. Fish, “Soft magnetic materials”, Proccedings of IEEE, 1990 vol 78 (6), pp. 947–972.

[111] G. Herzer, “Modern soft magnets: Amorphous and nanocrystalline materials”, ActaMaterialia,2013 vol61, pp. 718–734.

[112] D. Yuping, Z. Yahong, W. Tongmin, G. Shuchao, L. Xin, L. Xingjun, “Evolution study of microstructure and electromagnetic behaviors of Fe-Co-Ni alloy with mechanical alloying”, Materials Science and Engineering: B 185, 2014 vol, pp. 86–93.

[113] D. Weller, G.R. Harp, R.F.C. Farrow, A. Cebollada, J. Sticht, “Orientation dependence of the polar Kerr effect in Fcc and hcp Co”, Physical Review Letters,1994 vol72.